1. Introduction

Potassium bromate ($KBrO_3$) is used as in bread making a flour improver and in the production of fish-pastes. The EU countries now prohibit its use as a food additive because of its carcinogenicity. Japan and the USA, however, permit its use in bread making on the condition that it never remains in the final product. $KBrO_3$ causes tumors, especially in kidney, in rats, and mice after long-term oral administration in drinking water [1–3]. $KBrO_3$ is also genotoxic. It is positive in in vitro genotoxicity tests – including the bacterial reverse mutation assay [1], the chromosomal aberration test conducted in Chinese hamster cells [4], and the mouse lymphoma assay [5] – and in vivo in the micronucleus test (MN) [6,7].

It has been proposed that $KBrO_3$ induces tumors through the production of oxidative damage to DNA. Oxidative DNA damage can cause mutations that contribute to the activation of oncogenes and/or the inactivation of tumor suppressor genes, thereby leading to tumorigenesis [8,9]. 8-Hydroxydeoxyguanosine (8OHdG) is the main form of oxidative DNA damage induced by $KBrO_3$ [10]. It primarily causes GC > TA transversions (as a result of the pairing of 8OHdG with A) and is believed to be responsible for mutagenesis, carcinogenesis, and aging [11,12]. $KBrO_3$ increases 8OHdG DNA adducts in vivo and in vitro [13–15]. However, $KBrO_3$ induces mutations weakly in microbial mutation assays and the *Hprt* mutation assay in mammalian cells, while it induces chromosome aberrations strongly both in vivo and in vitro [1,16,17]. These findings raise the question of whether 8OHdG is required for the mutagenic process involved in $KBrO_3$-induced carcinogenesis.

In the present study, we examined the genotoxic properties of $KBrO_3$ using the comet assay (COM), the MN test, and thymidine kinase (*TK*) gene mutation assays in human lymphoblastoid TK6 cells [18]. Unlike the X-linked hemizygous *HPRT* gene mutation assay, the *TK* mutation assay can detect not only point mutations, but also large scale chromosomal deletions, recombinations, and aneuploidy [19–21]. Most of the genetic changes observed in *TK* mutants occur in human tumors and are presumed relevant to carcinogenesis. We analyzed the *TK* mutants induced by $KBrO_3$ at the molecular level and investigated what kind of mutation predominated. We also profiled global gene expression in TK6 cell exposed to $KBrO_3$ using Affymetrix GeneChip® Expression analysis to understand the genotoxic mechanism of $KBrO_3$.

2. Materials and methods

2.1. Cell culture, chemicals, and treatment

The TK6 human lymphoblastoid cell line has been described previously [22]. Cells were maintained in RPMI 1640 medium (Gibco-BRL, Life Technology Inc., Grand Island, NY) supplemented with 10% heat-inactivated horse serum (JR Biosciences, Lenexa, KS), 200 μg/ml sodium pyruvate, 100 U/ml penicillin, and 100 μg/ml streptomycin. The cultures were incubated at 37 °C in a 5% CO_2 atmosphere with 100% humidity. $KBrO_3$ (CAS No.7758-01-2) was purchased from Wako Pure Chemical Co. (Tokyo) and dissolved in RPMI medium just before use.

We prepared 20 ml aliquots of cell suspension at a concentration of 5.0×10^5 cells/ml in 50 ml polystyrene tubes. Different concentrations of $KBrO_3$ were added to the tubes, which were then placed on a platform shaker and incubated at 37 °C for 4 h with gentle shaking. At the end of the treatment period, the cell cultures were centrifuged, washed once, and re-suspended in fresh medium. We cultured them in new flasks for the MN assay and *TK* gene mutation assay, or diluted them for plating for survival estimates.

2.2. Genotoxicity assays

After treating cells with $KBrO_3$, we prepared slides for conducting the alkaline and neutral COM assay. The alkaline COM assay was performed as previously reported [23]. For the neutral COM assay, the slide was electrophoresed with chilled neutral solution (pH 8) containing of 90 mM Tris, 2 mM Na_2EDTA, and 90 mM boric acid according to the method by Wada et al. [24]. The COM slides were stained with SYBER green (Molecular Probes, Eugene, OR) and observed by an Olympus model BX50 fluorescence microscope. At least 50 cells were captured by CCD camera, and tail length of the comet was measured. The relationship between $KBrO_3$ treatment and migration was statistically analyzed by the Dunnett test [25].

We prepared the MN test samples 48 h after treatment, as previously reported [23]. Briefly, approximately 10^6 cells suspended in hypotonic KCl solution were incubated for 10 min at room temperature, fixed twice with ice-cold methanol containing 25% acetic acid, then re-suspended in methanol containing 1% acetic acid. A drop of the suspension was placed on a clean glass slide and air-dried. The cells were stained with 40 μg/ml acridine orange solution and immediately observed with the aid of an Olympus model BX50 fluorescence microscope equipped with a U-MWBV band pass filter. At least 1000 intact interphase cells for each treatment were examined, and the cells containing MN were scored. The MN frequencies between non-treated and treated cells were statistically analyzed by Fisher's exact test [26].

We prepared the *TK* gene mutation assay samples 3 days after treatment. We seeded cells from each culture into 96-well plates at 40,000 cells/well in the presence of 3.0 μg/ml trifluo-

rothymidine (TFT). We also plated 1.6 cells/well without TFT to determine plating efficiency. All plates were incubated at 37 °C in a humidified atmosphere of 5% CO_2 in air. After 14 days, we scored colonies on the PE plates and the normal-growing (NG) *TK* mutants on the TFT plates, then re-fed the plates containing TFT with fresh TFT, incubated them for an additional 14 days, and scored them for slow-growing (SG) *TK* mutants. Mutation frequencies, relative survival (RS), and relative suspension growth (RSG) were calculated as previously described [23]. The data of mutant frequencies were statistically analyzed by Omori's method, which consists of a modified Dunnett's procedure for identifying clear negative, a Simpson–Margolin procedure for detecting downturn data, and a trend test to evaluate the dose-dependency [27].

2.3. LOH analysis of TK mutations by polymerase chain reaction (PCR)

To avoid analyzing identical mutants, we performed an additional *TK* mutation assay and isolated *TK* mutants from independent culture after a 4 h treatment with 2.5 mM $KBrO_3$. We confirmed the phenotype of the *TK* mutant clones by re-challenging them with TFT medium. We also determined the growth rate of the clones and confirmed whether they were NG or SG mutants.

Genomic DNA was extracted from the *TK* mutant cells and used as a template for PCR. We conducted the PCR-based LOH analysis of the human *TK* gene as described previously [28]. A set of primers was used to each amplify the parts of exons 4 and 7 of the *TK* gene that is heterozygous for frame shift mutations. A third primer set for amplifying parts of the β-globin was also used as the internal control. We applied quantitative-multiple PCR for co-amplification of the three regions. The PCR products were analyzed with an ABI310 genetic analyzer (PE Biosystems, Chiba, Japan), and were classified into "no LOH", "hemizygous (hemi-) LOH", or "homozygous (homo-) LOH". To determine the extent of the LOH, we analyzed 10 microsatellite loci on chromosome 17q by PCR-based LOH analysis [28]. The results were processed by GenoTyper™ software (PE Biosystems, Chiba, Japan) according to the manufacturer's guidelines.

2.4. Gene expression analysis

Total RNA was isolated from the TK6 cells after 4 h treatment with 2.5 mM $KBrO_3$ and was purified by RNeasy columns (Qiagen, Valencia, CA). We conducted a single cDNA synthesis, cRNA labeling, and cRNA fragmentation according to the manufacturer's recommendations (Affymetrix Inc., Santa Clara, CA) and employed Affymetrix GeneChip Expression analysis. The hybridization mixture for each sample was hybridized to an Affymetrix U133A human genome array. We processed the scanned data using Microarray Suite Software Version 5.0 (Affymetrix Inc., Santa Clara, CA) and imported the data into GeneSpring software (Silicon Genetics, Redwood City, CA). Signal intensity was normalized by per-gene and per-chip, and the ratios were calculated by normalizing $KBrO_3$ sample to the corresponding control sample. We used intensity-dependent (step-wise) selection of significant changes with higher cut-off value for lower signal intensity (1.75-, 2.0-, 2.25-, 2.5-, and 3.5-fold for genes intensity range of >1000, 500–1000, 100–500, 50–100, and 10–50, respectively), and up-regulated genes with a presence call in $KBrO_3$ sample, whereas down-regulated genes with a presence call in the control sample.

3. Results

3.1. Cytotoxicity and genotoxicity of $KBrO_3$

$KBrO_3$ exerted strong and concentration-dependent cytotoxicity in TK6 cells (Fig. 1). It induced approximately 50% cytotoxicity (51% RSG and 44% RS) at 2.5 mM. To investigate whether $KBrO_3$ directly causes DNA damage, we conducted the COM assay. Induction of COM tail after the treatment of in alkaline version was statistically significant 2.5 and 5 mM. In the neutral COM assay, the induction was observed form the lower concentration (Fig. 1). Because the neutral COM is thought to be associated with DNA double strand breaks (DSBs) [29], this result indicates that $KBrO_3$ directly causes DNA damage including DSBs. $KBrO_3$ also induced MN and *TK* mutation in a concentration-dependent manner and their inductions were statistically significant (Fig. 1). At the maximum concentration, it induced both MN and *TK* mutation frequencies about 30 times the control values. Two distinct phenotypic classes of *TK* mutants were generated: NG mutants grew at the same rate as the wild type (doubling time 13–17 h), and SG mutants grew at a slower rate (doubling time > 21 h). NG mutants result from intragenic mutations, while SG mutants result from gross changes (extending beyond the *TK* gene) [20]. $KBrO_3$ predominantly induced SG mutants (Fig. 1), implying that $KBrO_3$ treatment predominantly causes gross structural changes, but not small genetic alterations such as point mutations.

3.2. Molecular analysis of TK mutants

The *TK* mutants were randomly isolated from independent cultures treated with 2.5 mM $KBrO_3$ for 4 h. Table 1 shows the cytotoxicity (RSG), mutation frequency, and proportion of SG mutants induced by $KBrO_3$. We subjected 40 induced mutants to LOH analysis. Of those, 32 (80%) were SG mutants, which corresponded closely to the percentage of SG mutants induced in the assay (74.1%), indicating that the result of LOH analysis reflected the character of the induced

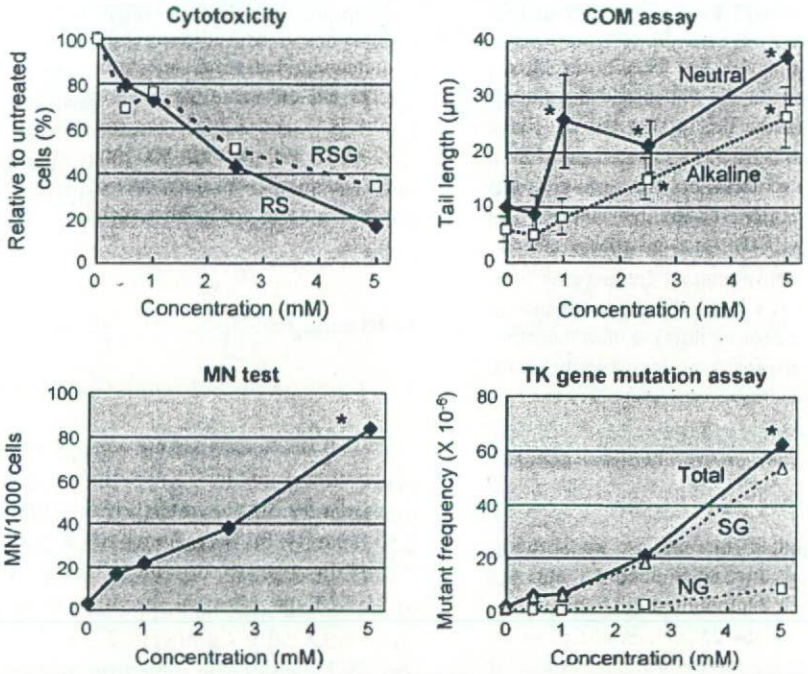

Fig. 1. Cytotoxic (relative survival, RS; relative suspension growth, RSG) and genotoxic responses (COM assay, MN test, and *TK* gene mutation assay) of TK6 cells treated with $KBrO_3$ for 4 h. Asterisk (*) statistically significant in Dunnett's test ($P < 0.05$) in COM assay, and in both pair-wise comparison and trend test ($P < 0.05$) in MN test and *TK* gene mutation assay.

mutations. Table 1 also shows the results of LOH analysis of the induced and spontaneously occurring mutants. The result of molecular analysis of spontaneous *TK* mutants was reported previously [21]. We classified the mutants into three types: non-LOH, hemizygous LOH (hemi-LOH), and homozygous LOH (homo-LOH). In general, hemi-LOH is resulted by deletion and homo-LOH is by inter-allelic homologous recombination [20]. Among the $KBrO_3$-induced mutants, 63% of NG mutants and 84% of SG mutants were hemi-LOH. In spontaneous mutants, on the other hand, majority of NG and SG mutants were non-LOH and homo-LOH, respectively. These results indicated that $KBrO_3$ predominantly induced large deletions. We previously reported the mutational spectra of *TK* mutants in TK6 cells that treated with the alkylating agent ethylmethane sulfonate (EMS), or X-irradiated [20,21]. Fig. 2 shows the comparison of the mutational spectra of spontaneous and induced *TK* mutants by EMS, X-irradiation, and $KBrO_3$. The mutation spectrum induced by $KBrO_3$ was similar to that induced by X-radiation (which also induces LOH, predominantly via deletion [21]) but not by EMS. The majority of the mutations induced by $KBrO_3$ were large deletions, but not point mutations.

Fig. 3 shows the regions of LOH and the distribution of spontaneous, X-ray-induced, and $KBrO_3$-induced

Table 1
Cytotoxic and mutational responses to $KBrO_3$, and the results of LOH analysis of normally growing (NG) and slowly growing (SG) *TK* mutants

Treatment	Cytotoxic and mutational response			LOH analysis at *TK* gene (%)			
	RSG (%)	MF ($\times 10^{-6}$)	% SG	Number	Non-LOH	Hemi-LOH	Homo-LOH
Spontaneous[a]	100	2.19	56	56			
NG mutants				19	14 (74)	3 (16)	2 (11)
SG mutants				37	0 (0)	9 (24)	28 (76)
$KBrO_3$ (2.5 mM)	51	29.4	74	39			
NG mutants				8	3 (37)	5 (63)	0 (0)
SG mutants				31	1 (3)	27 (84)	4 (13)

[a] Data from Zhan et al. [22].

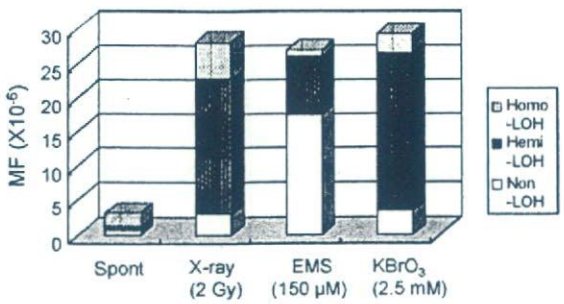

Fig. 2. *TK* mutation spectra in untreated, X-ray-treated (2 Gy), EMS-treated (150 μM, 4 h), and $KBrO_3$-treated (2.5 mM, 4 h) TK6 cells. The fraction of each mutational event was calculated by considering the ratio of NG to SG mutants and the results of molecular analysis (Table 1). The data for all but the $KBrO_3$ treatments were taken from our previous paper [20].

LOH mutants. $KBrO_3$ predominantly induced hemi-LOH, the result of large interstitial and terminal deletions, which we also frequently observed in the X-ray-induced LOH mutants. These results indicate that the genetic changes induced by $KBrO_3$ were similar to those induced by X-rays.

3.3. Gene expression analysis

Table 2 lists the genes that significantly increased expression following exposure to 2.5 mM $KBrO_3$. These genes are involved in stress response (6 genes), cell growth and DNA repair (19 genes), immune response (3 genes), apoptosis (3 genes), signal transduction (10 genes), transcription regulation (10 genes), chromosome organization (2 genes), protein modification (7 genes), energy metabolism (6 genes), lipid metabolism (2 genes), purine biosynthesis (3 genes), and unclassified functions (42 genes). Table 3 shows the genes whose expression was suppressed by the treatment. The number of up-regulated genes was greater that the number of down-regulated genes.

4. Discussion

$KBrO_3$ is a complete carcinogen, possessing both initiating and promoting activities in rodents [1]. While it shows clear positive responses in the COM assay, MN test, and chromosome aberration test using mammalian cells [4,14,17], the mutagenic potential of $KBrO_3$ in bacteria and the *Hprt* assay in Chinese hamster cells is weak or negative [1,14,17,30]. In our present study, $KBrO_3$ treatment strongly induced *TK* gene mutations. The reason we observed the induction of gene mutations and others did not is that $KBrO_3$ induces detectable mutagenecity in the *TK* gene but are only weakly mutagenic or non-mutagenic in the *Hprt* gene and in microbial assays [20]. The lower mutation frequency in the *Hprt* gene is due to the low recovery of large deletions, which are not detected because they are lethal. $KBrO_3$ is positive in mouse lymphoma cell assays that target the *Tk* gene [5]. In in vivo genotoxicity tests, $KBrO_3$ strongly induces MN in male ddY mice but is only weakly mutagenic in the *gpt* mutation assay in transgenic mice, which mainly detects point mutations and small deletions [31]. These results indicate that the property of genotoxicity

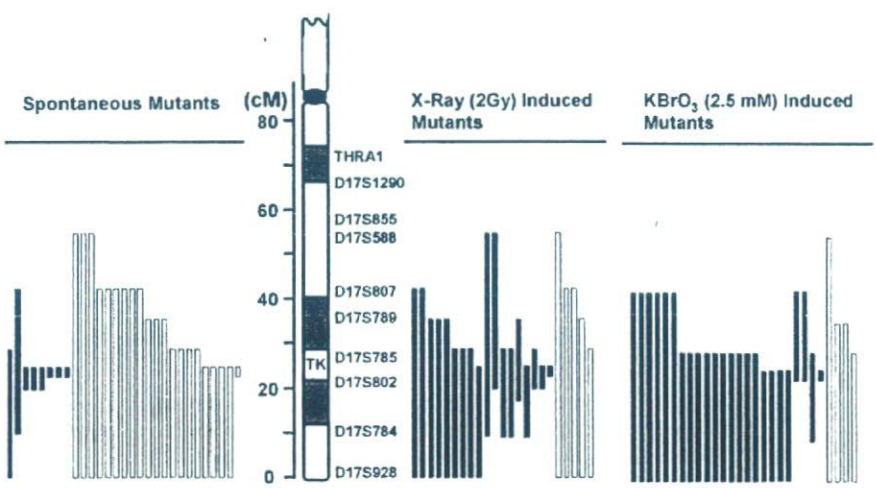

Fig. 3. The extent of LOH at the *TK* locus of TK6 cells that were untreated, X-ray-irradiated (2 Gy), or exposed to $KBrO_3$ (2.5 mM, 4 h). We examined 10 microsatellite loci on chromosome 17q that are heterozygous in TK6 cells. The human *TK* locus maps to 17q23.2. Open and closed bars represent homozygous LOH and hemizygous LOH, respectively. The length of the bar indicates the extent of the LOH. We analyzed 28 LOH mutants (4 NG and 24 SG). The data on spontaneous and X-ray-induced mutants were taken from our previous paper [20].

Table 2
Genes whose expression was up-regulated by $KBrO_3$ (2.5 mM, 4 h)

	Gene symbol	Ratio	Gene title
Stress response	CAT	2.77	Catalase
	DNAJC7	2.33	DnaJ (Hsp40) homolog, subfamily C, member 7
	FKBP5	2.87	FK506 binding protein 5
	HSPA8	3.02	Heat shock 70 kDa protein 8
	HSPCB	3.21	Heat shock 90 kDa protein 1, beta
	HSPD1	1.83	Heat shock 60 kDa protein 1
DNA repair, cell cycle, cell growth	BUB1	4.51	BUB1 budding uninhibited by benzimidazoles 1 homolog
	CCND2	5.08	Cyclin d2
	CCT2	3.33	Chaperonin containing TCP1, subunit 2 (beta)
	DKC1	2.37	Dyskeratosis congenita 1, dyskerin
	ENO1	2.10	Enolase 1 (alpha)
	HMGB1	2.16	High-mobility group box 1
	MAPRE1	2.32	Microtubule-associated protein, RP/EB family, member 1
	NME1	2.00	Non-metastatic cells 1, protein (NM23A) expressed in
	NOLC1	2.99	Nucleolar and coiled-body phosphoprotein 1
	NRAS	2.54	Neuroblastoma RAS viral (v-ras) oncogene homolog
	p21	3.22	Cyclin-dependent kinase inhibitor 1A (p21, Cip1)
	PPP2R1B	2.45	Protein phosphatase 2 (formerly 2A), regulatory subunit A (PR 65), beta isoform
	RAD21	2 34	RAD21 homolog
	RBBP4	2.00	Retinoblastoma binding protein 4
	RHOA	1.77	ras homolog gene family, member A
	SRPK1	2.75	SFRS protein kinase 1
	SSR1	2.66	Signal sequence receptor, alpha
Immune response	ARHGDIB	1.78	Rho GDP dissociation inhibitor (GDI) beta
	HLA-DRA	2.16	Major histocompatibility complex, class II, DR alpha
	IL2RG	2.43	Interleukin 2 receptor, gamma
Apoptosis	BCLAF1	6.42	BCL2-associated transcription factor 1
	FXR1	3.32	Fragile X mental retardation, autosomal homolog 1
	VDAC1	1.94	Voltage-dependent anion channel 1
Signal transduction	ANP32A	3.20	Acidic (leucine-rich) nuclear phosphoprotein 32 family, member A
	OGT	2.74	O-linked *N*-acetylglucosamine (GlcNAc) transferase
	PIP5K1A	4.25	Phosphatidylinositol-4-phosphate 5-kinase, type I, alpha
	PLEK	2.95	Pleckstrin
	PTPN11	2.61	Protein tyrosine phosphatase, non-receptor type 11
	SPTLC1	2.62	Serine palmitoyltransferase, long chain base subunit 1
	SRPR	2.52	Signal recognition particle receptor
Transcription regulation	CDC5L	4.37	CDC5 cell division cycle 5-like
	HNRPC	4.40	Heterogeneous nuclear ribonucleoprotein C (C1/C2)
	MED6	2.45	Mediator of RNA polymerase II transcription, subunit 6 homolog
	MED6	2.45	Mediator of RNA polymerase II transcription, subunit 6 homolog
	NO NO	2.68	Non-POU domain containing, octamer-binding
	POLR1C	2.67	Polymerase (RNA) I polypeptide C, 30 kDa
	PRPF4	2.51	PRP4 pre-mRNA processing factor 4 homolog
Chromosome organization	CBX5	2.68	Chromobox homolog 5 (HP1 alpha homolog, Drosophila)
Protein modification	CANX	2.56	Calnexin
	COPA	6.55	Coatomer protein complex, subunit alpha
	EIF2S3	2.40	Eukaryotic translation initiation factor 2, subunit 3 gamma
	EIF4B	2.86	Eukaryotic translation initiation factor 4B
	RANBP2	3.96	RAN binding protein 2
	SEC23IP	2.67	SEC23 interacting protein

Table 2 (*Continued*)

	Gene symbol	Ratio	Gene title
Energy pathway	AFURS1	2.83	ATPase family homolog up-regulated in senescence cells
	CYB5-M	2.54	Cytochrome *b*5 outer mitochondrial membrane precursor
	TOMM22	3.07	Translocase of outer mitochondrial membrane 22 homolog
Lipid metabolism	HMGCS1	2.58	3-Hydroxy-3-methylglutaryl-Coenzyme A synthase 1
	SCD	2.56	Stearovl-CoA desaturase
Purine biosynthesis	ENTPD1	2.36	Ectonucleoside triphosphate diphosphohydrolase 1
	GART	2.64	Phosphoribosylglycinamide formyltransferase
	PAICS	1.79	Phosphoribosylaminoimidazole carboxylase
Unclassified	BANF1	2.77	Barrier to autointegration factor 1
	BAT1	1.95	HLA-B associated transcript 1///HLA-B associated transcript 1
	C1orf16	2.37	Chromosome 1 open reading frame 16
	CALU	2.40	Calumenin
	DAZAP2	2.57	DAZ associated protein 2
	DDX18	2.34	DEAD (Asp-Glu-Ala-Asp) box polypeptide 18
	DHX9	9.37	DEAH (Asp-Glu-Ala-His) box polypeptide 9
	EXOSC2	3.03	Exosome component 2
	FLJ10534	2.07	Hypothetical protein FLJ10534
	FLJ10719	2.42	Hypothetical protein FLJ10719
	FLJ12973	2.76	Hypothetical protein FLJ12973
	GANAB	2.07	Glucosidase, alpha; neutral AB
	HEM1	2.37	Hematopoietic protein 1
	IGHM	2.76	Anti-HIV-1 gp120 V3 loop antibody DO142-10 light chain variable region
	IGKC	3.15	Anti-rabies virus immunoglobulin rearranged kappa chain V-region
	LIN7C	3.51	lin-7 homolog C (*C. elegans*)
	LOC54499	2.31	Putative membrane protein
	M6PR	3.59	Mannose-6-phosphate receptor
	MGC8902	2.27	Hypothetical protein MGC8902/
	MOBK1B	2.67	MOB1, Mps one binder kinase activator-like 1B (yeast)
	NS	2.15	Nucleostemin
	NUSAP1	3.25	Nucleolar and spindle associated protein 1
	OK/SW-cl.56	1.85	Beta 5-tubulin
	OPRS1	2.76	Opioid receptor, sigma 1
	PEG 10	2.50	Paternally expressed 10
	PEX19	2.34	Peroxisomal biogenesis factor 19
	PGK1	2.11	Phosphoglycerate kinase 1
	RPE	2.35	Ribulose-5-phosphate-3-epimerase
	SDBCAG84	3.16	Serologically defined breast cancer antigen 84
	SMU1	2.70	smu-1 suppressor of mec-8 and unc-52 homolog (*C. elegans*)
	TAGLN2	2.03	Transgelin 2
	UBC	2.65	Ubiquitin C
	XPNPEP1	2.84	X-prolyl aminopeptidase
	YWHAE	6.39	Tyrosine 3-monooxygenase/tryptophan 5-monooxygenase activation protein, epsilon polypeptide
	YWHAZ	2.50	Tyrosine 3-monooxygenase/tryptophan 5-monooxygenase activation protein, zeta polypeptide

of $KBrO_3$ predominantly causes gross structural changes rather than small genetic changes such as point mutations.

$KBrO_3$ generates high yields of 8OHdG DNA adducts, which is a marker of oxidative DNA damage widely used as a predictor of carcinogenesis [10]. 8OHdG has been reported to be highly mutagenic in some experiments. In cell-free system, 8OHdG induced mutation by misincorporating adenine instead of cytosine [12]. Artificially incorporated 8OHdG at specific codons in a shuttle vector system efficiently induced GC > TA transversions in mammalian cells and *E. coli* [8,32,33]. In mammalian gene mutation assays in vitro and in vivo, however, the relationship between the accumulation of 8OHdG and the induction of GC > TA transversion has not been clear. Takeuchi et al.

Table 3
Genes whose expression was down-regulated by $KBrO_3$ (2.5 mM, 4 h)

	Gene symbol	Ratio	Gene title
Cell cycle, cell growth	FH	0.51	Fumarate hydratase
	MYC	0.55	v-myc myelocytomatosis viral oncogene homolog
Signal transduction	DUSP2	0.37	Dual specificityphosphatase 2
	RRBP1	0.39	Ribosome binding protein 1 homolog 180 kDa
	TBL3	0 43	Transducin (beta)-like3
Transcription regulation	CITED2	0.45	Cbp/p300-interacting transactivator, with Glu/Asp-rich carboxy-terminal domain, 2
	KIAA1196	0.43	KIAA1196 protein
	TZFP	0 39	Testis zinc finger protein
Chromosome organization	H1FX	0.14	H1 histone family member X
Protein modification	CLTB	0.43	Clathrin, light polypeptide (Lcb)
Energy pathway	FDX1	0.45	Ferredoxin 1
	QPRT	0.41	Quinolinate phosphoribosyltransferase
	SLC39A4	0.43	Solute carrier family 39 (zinc transporter), member 4
Unclassified	BTBD2	0.35	BTB (POZ) domain containing 2
	LOC339229	0.44	Hypothetical protein LOC339229
	MGRN1	0.44	Mahogunin, ring finger 1
	MRP63	0.41	Mitochondrial ribosomal protein 63
	PHLDA1	0.43	Pleckstrin homology-like domain, family A, member 1
	PTPLA	0.37	Protein tyrosine phosphatase-like (proline instead of catalytic arginine), member a
	SPATA2	0.45	Spermatogenesis associated 2

examined the mutagenicity of a hydroxyl radical generator, *N,N'*-bis (2-hydroxyperoxy-2-methoxyethyl)-1,4,5,8-naphthalene-tetra-carboxylic diimide (NP-III). Although NP-III highly produced 8OHdG upon irradiation with UV in V79 cells, the frequency of *Hprt* gene mutation was not significantly induced [34]. Molecular analysis demonstrated the no association of induction of 8OHdG with GC > TA transversion in the *Hprt* mutants [35]. 8OHdG is mainly removed by Ogg1 protein in a manor of the base excision repair (BER) pathway. Arai et al. investigated the relationship between the accumulation of oxidative DNA damage and the induction of gene mutation using *Ogg*1 deficient transgenic mice [36]. Although the 8OHdG level in kidneys of the *Ogg*1 deficient mice increase 200 times of the control level after 4 weeks' $KBrO_3$ treatment, the mutation frequency in the transgenic *gpt* gene was induced by less than 10 times of the control level. The molecular analysis revealed that the fraction of GC > TA transversions did not specifically increased. These results suggest that 8OHdG-mediated base substitutions do not mainly contribute to the mutagenic process involved in $KBrO_3$-induced carcinogenesis. Other genotoxic events must be involved in the carcinogenic process.

Our present studies strongly support this hypothesis. We demonstrated that $KBrO_3$ treatment clearly induced DNA damage in both the alkaline and neutral COM assay (Fig. 1). The alkaline COM assay is capable of detecting any DNA damages including DSB, single strand breaks (SSB), alkali-labile sites, DNA–DNA/DNA–protein cross-linking, and SSB associated with incomplete excision repair sites, while the neutral COM assay allows the detection of DSB, considered to be "biologically relevant" lesion of radiation damage [24]. $KBrO_3$ may have radio-mimic genotoxicity that yields oxidative DNA damage as well as DSB. $KBrO_3$ also induced MN formation and *TK* gene mutation significantly in TK6 cells. In the *TK* gene mutation assay, $KBrO_3$ predominantly produced SG mutants, but not NG mutants (Fig. 1c), implying that gross structural changes such as deletion and recombination are associated with the mutations. Molecular analysis of the *TK* mutants confirmed the assumption. Most of *TK* mutants showed LOH mutations, not non-LOH mutations, which are mainly point mutations. Harrington-Brock et al. also demonstrated that bromate compounds significantly induced *Tk* mutations in mouse lymphoma L5178Y cells, and almost all were LOH mutations [5]. LOH can be caused by deletions,

mitotic recombination between homologous alleles, or whole chromosome loss [20]. Molecular analysis can distinguish between them and reveal the mechanism and the characteristics of the mutants. In this study, $KBrO_3$ predominantly induced large deletions that resulted in hemizygous LOH (Table 1). The large deletions were mainly terminal deletions in the proximal region of chromosome 17q, which were rarely observed in spontaneously arising *TK* mutants (Fig. 3). The mutational spectrum and LOH pattern induced by $KBrO_3$ were similar to those induced by X-irradiation (Figs. 2 and 3) [20,21]. DSBs induced X-rays cause large deletions [19,20]. When the DSBs are repaired by the non-homologous end-joining pathway, interstitial deletions result. The broken chromosome ends can be also stabilized by the addition of new telomere sequences. Because TK6 cells have high telomerase activity [20], the result is terminal deletions. Thus, the major genotoxicity of $KBrO_3$ may be due to DSBs, but not to 8OHdG converting GC > TA transversion.

Some 8OHdG lesions can convert DSBs through the BER pathway [37]. In the initial step of BER, Ogg1 removes 8OHdG by DNA glycosylase activity and nicks the DNA backbone because of its associated lyase activity. The resulting SSB is processed by an apurinic endonuclease, which generates a single nucleotide gap. The gap is filled in by a DNA polymerase and sealed by a DNA ligase [38]. Clustered 8OHdG lesions induced by $KBrO_3$ may not be appropriately repaired by BER and cause DSB, however, because it is possible that two closely opposed 8OHdGs convert two closely opposed SSBs by BER resulting DSB [39,40]. Yang et al. developed Ogg1 over-expressing TK6 cell (TK6-hOGG1) and examined cytotoxic and mutagenic responses to gamma-irradiation [41]. They demonstrated that TK6-hOGG1 cells are more sensitive than the parental TK6 cells to cytotoxicity and mutagenicity by gamma-irradiation, and most of the induced *TK* mutants in TK6-OGG1 exhibited SG phenotype, which were probably large deletion mutants resulted by DSBs. This result clearly indicates that BER pathway contributes to convert oxidative damages to DSBs. Some clustered 8OHdG induced by $KBrO_3$ may covert to DSBs in TK6 cells, because TK6 is Ogg1 proficient cells [37].

To clarify the genotoxic characteristics of $KBrO_3$, we investigated the gene expression profile using Affymetrix GeneChip® Expression analysis. Many genes were up- or down-regulated by exposure to 2.5 mM $KBrO_3$ (Tables 2 and 3). Akerman et al. investigated the alterations of gene expression profiles in ionizing radiation-exposed TK6 cells [42]. They reported a >50% increase in expression of ATF-3 (stress response), Cyclin G (cell cycle), FAS antigen (apoptosis), GADD45 (repair and apoptosis), PCNA (repair), Rad51 (repair), and p21 (cell cycle) and a 40% decrease in expression of c-Myc (transcription factor), interferon stimulatory gene factor-3 (cell signaling), and p55CDC (cell cycle). We also observed up-regulation of p21 and down-regulation of c-Myc. Up-regulation of p21, however, is observed in TK6 cells exposed to any DNA-damaging chemical [43]. Islaih et al. also demonstrated the relationship between the gene expression profiles and the DNA damaging agents using TK6 cells [43]. They examined six chemicals including H_2O_2 and bleomycin which induce oxidative DNA damage. Although 10 genes were commonly up-regulated between H_2O_2 and bleomycin treatments, these genes except for p21 were not observed in our experiment. Thus, we could not find the similarity of gene expression profile by the treatment with $KBrO_3$ to by the treatment with ionizing radiation as well as oxidative damage inducers. Comparing gene expression profiles across platforms, laboratories, and experiments must be difficult [44]. Although it is difficult to judge from the expression analysis of the single chemical, information on genes which altered their expression gives a clue to understand the mechanism of action. Firstly, predominance of DNA repair and cell cycle related genes in up-regulated genes supports the genotoxic action of $KBrO_3$. Up-regulation of stress genes and apoptosis related genes suggests an involvement of oxidative stress. Up-regulation of catalase may be responsible for the oxidative damage by $KBrO_3$ (Table 2). Unclassified genes for alteration may have a functional relationship with genotoxic mechanism.

In conclusion, $KBrO_3$ predominantly induced large deletions at chromosomal level in human TK6 cells. The major genotoxicity leading to carcinogenesis of $KBrO_3$ may be due to DSBs rather than to 8OHdG adducts that lead to GC > TA transversions, as is commonly believed.

Acknowledgments

The TK6 cell line used in this study was a kind gift of Dr. John B. Little of the Harvard School of Public Health, Boston, MA. This study was supported by Health, Welfare, and Labor Science Research Grants (H15-chem-002, H15-food-004) in Japan.

References

[1] Y. Kurokawa, A. Maekawa, M. Takahashi, Y. Hayashi, Toxicity and carcinogenicity of potassium bromate—a new renal carcinogen, Environ. Health Perspect. 87 (1990) 309–335.

[2] Y. Kurokawa, S. Aoki, Y. Matsushima, N. Takamura, T. Imazawa, Y. Hayashi, Dose–response studies on the carcinogenicity of potassium bromate in F344 rats after long-term oral administration, J. Natl. Cancer Inst. 77 (1986) 977–982.
[3] A.B. DeAngelo, M.H. George, S.R. Kilburn, T.M. Moore, D.C. Wolf, Carcinogenicity of potassium bromate administered in the drinking water to male B6C3F1 mice and F344/N rats, Toxicol. Pathol. 26 (1998) 587–594.
[4] M. Ishidate Jr., K. Yoshikawa, Chromosome aberration tests with Chinese hamster cells in vitro with and without metabolic activation—a comparative study on mutagens and carcinogens, Arch. Toxicol. Suppl. 4 (1980) 41–44.
[5] K. Harrington-Brock, D.D. Collard, T. Chen, Bromate induces loss of heterozygosity in the thymidine kinase gene of L5178Y/Tk(±)-3.7.2C mouse lymphoma cells, Mutat. Res. 537 (2003) 21–28.
[6] M. Hayashi, T. Sofuni, M. Ishidate Jr., High-sensitivity in micronucleus induction of a mouse strain (MS), Mutat. Res. 105 (1982) 253–256.
[7] M. Hayashi, M. Kishi, T. Sofuni, M. Ishidate Jr., Micronucleus tests in mice on 39 food additives and eight miscellaneous chemicals, Food Chem. Toxicol. 26 (1988) 487–500.
[8] H. Kamiya, K. Miura, H. Ishikawa, H. Inoue, S. Nishimura, E. Ohtsuka, c-Ha-ras containing 8-hydroxyguanine at codon 12 induces point mutations at the modified and adjacent positions, Cancer Res. 52 (1992) 3483–3485.
[9] A.G. Knudson, Antioncogenes and human cancer, Proc. Natl. Acad. Sci. U.S.A. 90 (1993) 10914–10921.
[10] H. Kasai, S. Nishimura, Y. Kurokawa, Y. Hayashi, Oral administration of the renal carcinogen, potassium bromate, specifically produces 8-hydroxydeoxyguanosine in rat target organ DNA, Carcinogenesis 8 (1987) 1959–1961.
[11] K.C. Cheng, D.S. Cahill, H. Kasai, S. Nishimura, L.A. Loeb, 8-Hydroxyguanine, an abundant form of oxidative DNA damage, causes G–T and A–C substitutions, J. Biol. Chem. 267 (1992) 166–172.
[12] S. Shibutani, M. Takeshita, A.P. Grollman, Insertion of specific bases during DNA synthesis past the oxidation-damaged base 8-oxodG, Nature 349 (1991) 431–434.
[13] K. Sai, C.A. Tyson, D.W. Thomas, J.E. Dabbs, R. Hasegawa, Y. Kurokawa, Oxidative DNA damage induced by potassium bromate in isolated rat renal proximal tubules and renal nuclei, Cancer Lett. 87 (1994) 1–7.
[14] G. Speit, S. Haupter, P. Schutz, P. Kreis, Comparative evaluation of the genotoxic properties of potassium bromate and potassium superoxide in V79 Chinese hamster cells, Mutat. Res. 439 (1999) 213–221.
[15] T. Umemura, K. Sai, A. Takagi, R. Hasegawa, Y. Kurokawa, A possible role for oxidative stress in potassium bromate (KBrO3) carcinogenesis, Carcinogenesis 16 (1995) 593–597.
[16] K. Fujie, H. Shimazu, M. Matsuda, T. Sugiyama, Acute cytogenetic effects of potassium bromate on rat bone marrow cells in vivo, Mutat. Res. 206 (1988) 455–458.
[17] M. Ishidate Jr., T. Sofuni, K. Yoshikawa, M. Hayashi, T. Nohmi, M. Sawada, A. Matsuoka, Primary mutagenicity screening of food additives currently used in Japan, Food Chem. Toxicol. 22 (1984) 623–636.
[18] H.L. Liber, W.G. Thilly, Mutation assay at the thymidine kinase locus in diploid human lymphoblasts, Mutat. Res. 94 (1982) 467–485.
[19] H.L. Liber, D.W. Yandell, J.B. Little, A comparison of mutation induction at the tk and hprt loci in human lymphoblastoid cells; quantitative differences are due to an additional class of mutations at the autosomal tk locus, Mutat. Res. 216 (1989) 9–17.
[20] M. Honma, Generation of loss of heterozygosity and its dependency on p53 status in human lymphoblastoid cells, Environ. Mol. Mutagen. 45 (2005) 162–176.
[21] M. Honma, M. Hayashi, T. Sofuni, Cytotoxic and mutagenic responses to X-rays and chemical mutagens in normal and p53-mutated human lymphoblastoid cells, Mutat. Res. 374 (1997) 89–98.
[22] L. Zhan, H. Sakamoto, M. Sakuraba, D.S. Wu, L.S. Zhang, T. Suzuki, M. Hayashi, M. Honma, Genotoxicity of microcystin-LR in human lymphoblastoid TK6 cells, Mutat. Res. 557 (2004) 1–6.
[23] N. Koyama, H. Sakamoto, M. Sakuraba, T. Koizumi, Y. Takashima, M. Hayashi, H. Matsufuji, K. Yamagata, S. Masuda, N. Kinae, M. Honma, Genotoxicity of acrylamide and glycidamide in human lymphoblastoid TK6 cells, Mutat. Res. 603 (2006) 151–158.
[24] S. Wada, H. Kurahayashi, Y. Kobayashi, T. Funayama, K. Yamamoto, M. Natsuhori, N. Ito, The relationship between cellular radiosensitivity and radiation-induced DNA damage measured by the comet assay, J. Vet. Med. Sci. 65 (2003) 471–477.
[25] M. Watanabe-Akanuma, T. Ohta, Y.F. Sasaki, A novel aspect of thiabendasole as a photomutagen in bacteria and cultured human cells, Mutat. Res. 158 (2005) 213–219.
[26] T. Matsushima, M. Hayashi, A. Matsuoka, M. Ishidate Jr., K.F. Miura, H. Shimizu, Y. Suzuki, K. Morimoto, H. Ogura, K. Mure, K. Koshi, T. Sofuni, Validation study of the in vitro micronuclei test in a Chinese hamster lung cell line (CHL/IU), Mutagenesis 14 (1999) 569–580.
[27] T. Omori, M. Honma, M. Hayashi, Y. Honda, I. Yoshimura, A new statistical method for evaluating of L5178Ytk± mammalian cell data using microwell method 517 (2002) 199–208.
[28] M. Honma, M. Momose, H. Tanabe, H. Sakamoto, Y. Yu, J.B. Little, T. Sofuni, M. Hayashi, Requirement of wild-type p53 protein for maintenance of chromosomal integrity, Mol. Carcinog. 28 (2000) 203–214.
[29] P.L. Olive, DNA damage and repair in individual cells: applications of the comet assay in radiobiology, Int. J. Radiat. Biol. 75 (1999) 395–405.
[30] D.E. Levin, M. Hollstein, M.F. Christman, E.A. Schwiers, B.N. Ames, A new Salmonella tester strain (TA102) with A X T base pairs at the site of mutation detects oxidative mutagens, Proc. Natl. Acad. Sci. U.S.A. 79 (1982) 7445–7449.
[31] T. Arai, V.P. Kelly, O. Minowa, T. Noda, S. Nishimura, High accumulation of oxidative DNA damage, 8-hydroxyguanine, in Mmh/Ogg1 deficient mice by chronic oxidative stress, Carcinogenesis 23 (2002) 2005–2010.
[32] F. Le Page, A. Margot, A.P. Grollman, A. Sarasin, A. Gentil, Mutagenicity of a unique 8-oxoguanine in a human Ha-ras sequence in mammalian cells, Carcinogenesis 16 (1995) 2779–2784.
[33] M.L. Wood, M. Dizdaroglu, E. Gajewski, J.M. Essigmann, Mechanistic studies of ionizing radiation and oxidative mutagenesis: genetic effects of a single 8-hydroxyguanine (7-hydro-8-oxoguanine) residue inserted at a unique site in a viral genome, Biochemistry 29 (1990) 7024–7032.
[34] T. Takeuchi, S. Matsugo, K. Morimoto, Mutagenicity of oxidative DNA damage in Chinese hamster V79 cells, Carcinogenesis 18 (1997) 2051–2055.
[35] M. Nakajima, T. Takeuchi, K. Ogino, K. Morimoto, Lack of direct involvement of 8-hydroxy-2′-deoxyguanosine in

hypoxanthine-guanine phosphoribosyltransferase mutagenesis in V79 cells treated with *N,N'*-bis(2-hydroxyperoxy-2-methoxyethyl)-1,4,5,8-naphthalenetetracarboxyli c-diimide (NP-III) or riboflavin, Jpn. J. Cancer Res. 93 (2002) 247–252.

[36] T. Arai, V.P. Kelly, K. Komoro, O. Minowa, T. Noda, S. Nishimura, Cell proliferation in liver of Mmh/Ogg1-deficient mice enhances mutation frequency because of the presence of 8-hydroxyguanine in DNA, Cancer Res. 63 (2003) 4287–4292.

[37] N. Yang, M.A. Chaudhry, S.S. Wallace, Base excision repair by hNTH1 and hOGG1: a two edged sword in the processing of DNA damage in gamma-irradiated human cells, DNA Repair (Amst.) 5 (2006) 43–51.

[38] G. Slupphaug, B. Kavli, H.E. Krokan, The interacting pathways for prevention and repair of oxidative DNA damage, Mutat. Res. 531 (2003) 231–251.

[39] K. Tian, M. McTigue, S.C. de los, Sorting the consequences of ionizing radiation: processing of 8-oxoguanine/abasic site lesions, DNA Repair (Amst.) 1 (2002) 1039–1049.

[40] M.E. Lomax, S. Cunniffe, P. O'Neill, Efficiency of repair of an abasic site within DNA clustered damage sites by mammalian cell nuclear extracts, Biochemistry 43 (2004) 11017–11026.

[41] N. Yang, H. Galick, S.S. Wallace, Attempted base excision repair of ionizing radiation damage in human lymphoblastoid cells produces lethal and mutagenic double strand breaks, DNA Repair (Amst.) 3 (2004) 1323–1334.

[42] G.S. Akerman, B.A. Rosenzweig, O.E. Domon, C.A. Tsai, M.E. Bishop, L.J. McGarrity, J.T. Macgregor, F.D. Sistare, J.J. Chen, S.M. Morris, Alterations in gene expression profiles and the DNA-damage response in ionizing radiation-exposed TK6 cells, Environ. Mol. Mutagen. 45 (2005) 188–205.

[43] M. Islaih, B.W. Halstead, I.A. Kadura, B. Li, J.L. Reid-Hubbard, L. Flick, J.L. Altizer, D.J. Thom, D.K. Monteith, R.K. Newton, D.E. Watson, Relationships between genomic, cell cycle, and mutagenic responses of TK6 cells exposed to DNA damaging chemicals, Mutat. Res. 578 (2005) 100–116.

[44] C.L. Yauk, M.L. Berndt, A. Williams, G.R. Douglas, Comprehensive comparison of six microarray technologies, Nucleic Acids Res. 32 (2004) e124.

Neuroscience 147 (2007) 153–163

RETINOIC ACIDS ACTING THROUGH RETINOID RECEPTORS PROTECT HIPPOCAMPAL NEURONS FROM OXYGEN-GLUCOSE DEPRIVATION-MEDIATED CELL DEATH BY INHIBITION OF C-JUN-N-TERMINAL KINASE AND p38 MITOGEN-ACTIVATED PROTEIN KINASE

Y. SHINOZAKI,[a] Y. SATO,[b]* S. KOIZUMI,[a] Y. OHNO,[c] T. NAGAO[c] AND K. INOUE[d]

[a]*Division of Pharmacology, National Institute of Health Sciences, 1-18-1 Kamiyoga, Setagaya, Tokyo 158-8501, Japan*

[b]*Division of Cellular and Gene Therapy Products, National Institute of Health Sciences, 1-18-1 Kamiyoga, Setagaya, Tokyo 158-8501, Japan*

[c]*National Institute of Health Sciences, 1-18-1 Kamiyoga, Setagaya, Tokyo 158-8501, Japan*

[d]*Department of Molecular and System Pharmacology, Graduate School of Pharmaceutical Sciences, Kyushu University, Maidashi3-1-1, Higashi-ku, Fukuoka 812-8582, Japan*

Abstract—Retinoic acids (RAs), including all-*trans* retinoic acid (ATRA) and 9-*cis* retinoic acid (9-*cis* RA), play fundamental roles in a variety of physiological events in vertebrates, through their specific nuclear receptors: retinoic acid receptor (RAR) and retinoid X receptor (RXR). Despite the physiological importance of RA, their functional significance under pathological conditions is not well understood. We examined the effect of ATRA on oxygen/glucose-deprivation/reperfusion (OGD/Rep)-induced neuronal damage in cultured rat hippocampal slices, and found that ATRA significantly reduced neuronal death. The cytoprotective effect of ATRA was observed not only in cornu ammonis (CA) 1 but also in CA2 and dentate gyrus (DG), and was attenuated by selective antagonists for RAR or RXR. By contrast, in the CA3 region, no protective effects of ATRA were observed. The OGD/Rep also increased phosphorylated forms of c-jun-N-terminal kinase (P-JNK) and p38 (P-p38) in hippocampus, and specific inhibitors for these kinases protected neurons. ATRA prevented the increases in P-JNK and P-p38 after OGD/Rep, as well as the decrease in NeuN and its shrinkage, all of which were inhibited by antagonists for RAR or RXR. These findings suggest that the ATRA signaling via retinoid receptors results in the inhibition of JNK and p38 activation, leading to the protection of neurons against OGD/Rep-induced damage in the rat hippocampus.

*Corresponding author. Tel: +81-3-3700-1141x275; fax: +81-3-3707-6950.
E-mail address: yoji@nihs.go.jp (Y. Sato).

Abbreviations: ATRA, all-*trans* retinoic acid; CA, cornu ammonis; DG, dentate gyrus; ERK, extracellular signal-regulated kinase; Hanks' BSS, Hanks' balanced salt solution; JNK, c-jun-N-terminal kinase; MAPK, mitogen-activated protein kinase; MKP-1, mitogen-activated protein kinase phosphatase-1; OGD, oxygen and glucose deprivation; PBS-T, phosphate-buffered saline with 0.3% Triton X-100, pH 7.6; P-ERK, phosphorylated extracellular signal-regulated kinase; PI, propidium iodide; P-JNK, phosphorylated c-jun-N-terminal kinase; P-p38, phosphorylated p38; RA, retinoic acid; RAR, retinoic acid receptor; Rep, reperfusion; RXR, retinoid X receptor; ssDNA, single-stranded DNA; TBS/T, Tris-buffered saline containing 0.1% Tween-20; 9-*cis* RA, 9-*cis* retinoic acid.

Key words: retinoic acid, RAR, RXR, MAPK, ischemia.

Retinoids, including vitamin A (retinol) and its derivatives, regulate a wide range of biological processes, such as cell growth and differentiation, development, and carcinogenesis (Chambon, 1996; Maden, 2001). Retinoic acids (RAs) regulate the expression of a large number of genes upon binding and activation of the nuclear retinoid receptors, retinoic acid receptors (RARα, RARβ, and RARγ) and retinoid X receptors (RXRα, RXRβ, and RXRγ) (Chambon, 1996; Maden, 2001). RARs are activated by all-*trans* retinoic acid (ATRA) and 9-*cis* retinoic acid (9-*cis* RA), whereas RXRs are activated by 9-*cis* RA (Chambon, 1996) and other non-retinoid lipid ligands such as docosahexaenoic acid (de Urquiza et al., 2000). In the presence of RA, these receptors act as transcription factors in forms of RAR/RXR heterodimers or RXR homodimers, which bind to retinoic acid response elements (RARE) in the promoter of target genes (Chambon, 1994; Kastner et al., 1997). RA has multiple effects on physiological functions in the adult brain, such as long-term potentiation and long-term depression (Chiang et al., 1998; Misner et al., 2001) and neurogenesis (Haskell and LaMantia, 2005; Jacobs et al., 2006). RA also plays significant roles under pathological conditions. For example, in mesangial cells and fibroblast, ATRA has a protective effect against H_2O_2 via receptor-mediated mechanisms (Konta et al., 2001; Xu et al., 2002). Although several lines of evidence link RA to some psychiatric pathogenesis (Strahan and Raimer, 2006), defects in retinoid signaling have been associated with neurodegenerative disorders such as Alzheimer's disease and amyotrophic lateral sclerosis (Corcoran et al., 2002; Goodman and Pardee, 2003). However, the role of RA signaling in other pathological conditions such as ischemia in the brain remains unclear.

The mitogen-activated protein kinase (MAPK) family, which plays an essential role in the transduction of environmental stimuli to the nucleus, consists of three commonly recognized subgroups: extracellular signal-regulated kinase (ERK), c-jun-N-terminal kinase (JNK), also known as the stress activated protein kinase (SAPK) and p38 kinase. JNK and p38 kinase are activated in response to cellular stresses like ischemia in the heart, kidney and brain (Hu and Wieloch, 1994; Mizukami et al., 1997; Yin et al., 1997; Herdegen et al., 1998; Walton et al., 1998) and have been associated with neuronal cell death (Xia et al., 1995; Watson et al., 1998; Namgung and Xia, 2000). JNK

0306-4522/07$30.00+0.00
doi:10.1016/j.neuroscience.2007.04.032

and p38 kinase activate downstream molecules such as caspase-3 (Kuan et al., 2003; Lee and Lo, 2003), Bax (Okuno et al., 2004), MAPK-activated protein kinase 2 (MAPKAP2) (Wang et al., 2002) and activator protein-1 (AP-1) (Ishikawa et al., 1997; Yokoo and Kitamura, 1997; Behrens et al., 1999) thereby leading of neuronal cell death. In contrast, ERK1/2 is mainly activated by various neurotransmitters, hormones and growth factors, controlling transcription factor activity to induce various physiological responses, such as cell proliferation or differentiation (Boulton et al., 1991; Marshall, 1995; Segal and Greenberg, 1996). However, ERK1/2 is also activated by various types of stress such as oxidative or shear stress, controlling the survival of cells (Xia et al., 1995; Guyton et al., 1996; Wang et al., 1998). Recent studies have shown that ATRA protects neurons from amyloidβ (Sahin et al., 2005) and staurosporine (Ahlemeyer and Krieglstein, 1998). Based on the findings above, we hypothesized that RA signaling would be inversely associated with neuronal cell death under pathological conditions. To test our hypothesis, we examined the effect of ATRA on hippocampal neurons against oxygen and glucose deprivation/reperfusion (OGD/Rep)-induced neuronal damage, and found that ATRA protected hippocampal neurons against cell death. We also found that the neuroprotective effect of ATRA was mediated by inhibition of OGD/Rep-induced activation of JNK and p38 kinase.

EXPERIMENTAL PROCEDURES

Materials

Propidium iodide (PI) and anti-β-actin antibody were purchased from Sigma Chemical Co. (St. Louis, MO, USA). The sources of the following chemicals are shown in parentheses: ATRA and 9-*cis* RA (Wako Pure Chemicals, Osaka, Japan), U0126, SB203580, SP600125 and anti-NeuN antibody (Calbiochem Biosciences, Inc., San Diego, CA, USA). LE135 (Li et al., 1999) and HX531 (Ebisawa et al., 1999) were synthesized and graciously provided by Dr. Koichi Shudo (Research Foundation Itsuu Laboratory, Tokyo, Japan). Antibodies against phosphorylated extracellular signal-regulated kinase 1/2 (P-ERK1/2), phosphorylated p38 (P-p38), phosphorylated c-jun-N-terminal kinase (P-JNK), and active caspase-3 were purchased from Cell Signaling Technology (Beverly, MA, USA). The sources of the following antibodies are shown in parentheses: single-stranded DNA (ssDNA) antibody (DAKO Cytomation, Glostrup, Denmark), RAR and RXR antibodies (Santa Cruz Biotechnology, Inc., Santa Cruz, CA, USA).

Organotypic hippocampal slice culture

Organotypic slice cultures of the hippocampus were prepared using the culture method described by Skrede and Westgaard (1971) All animals were treated in accordance with the laboratory animal care guidance of the National Institute of Health Sciences at Tokyo and the guidelines of the International Council for Laboratory Animal Science (ICLAS; http://www.iclas.org/). Every effort was made to minimize the number of experimental animals used and their suffering. Eleven-day-old Wistar rats were decapitated, and the brains were rapidly dissected and placed in a Petri dish containing ice-cold 1× Hanks' balanced salt solution (Hanks' BSS, from Gibco, Rockville, MD, USA). Both right and left hippocampi were isolated and sectioned into 300 μm transverse slices with a McIlwain tissue chopper (Mickle Laboratory Engineering Co. Ltd., Goose Green, UK). The slices were then carefully separated and transferred onto porous membrane inserts of six-well culture plates (two or three slices per insert) (Millicell-CM, Millipore, Billerica, MA, USA). To reach the level of insert membrane, 800 μL culture medium was added to the lower compartment of each well, and the culture plates were then placed in a 37 °C humidified incubator enriched with 5% CO_2. The cell culture medium consisted of 50% Minimum Essential Medium with 25 mM Hepes, 25% Hanks' BSS and 25% heat-inactivated horse serum, which were supplemented with 2 mM L-glutamine, 100 U/mL penicillin and 100 μg/mL streptomycin. On the next day, the culture medium was replaced with fresh medium and from then on changed once every 2 days. Hippocampal slices were used for each experiment after incubation for 12 days.

OGD

Hippocampal slices were exposed to OGD using an anaerobic chamber. The slices were transferred in dishes with 800 μl glucose-free DMEM containing (mg/L): 200 $CaCl_2$, 400 KCl, 97.67 $MgSO_4$, 6400 NaCl, 3700 $NaHCO_3$, 125 NaH_2PO_4 and then placed into an airtight chamber containing 95% N_2, 5% CO_2 (37 °C) for 40 min. After OGD, the slices were placed back in the incubator in normal culture medium and incubated for 24 h. RAs were added to the culture medium 24 h before OGD and during Rep. Antagonists for RAR and RXR were added to the medium 30 min before and during the RA treatment. Inhibitors of MAPKs were added to the slices simultaneously at Rep.

Immunohistochemistry

The hippocampal slices were fixed with 4% paraformaldehyde for 1–2 h and rinsed two times (each 10 min at room temperature) with PBS-T (phosphate-buffered saline with 0.3% Triton X-100, pH 7.6). After blocking with 3% normal goat serum in PBS-T for 2 h at room temperature, the slices were incubated with the primary antibody (1/1000-fold dilution in PBS-T with 3% goat serum) for 48 h at 4 °C, followed by incubation with the Alexa Fluor-conjugated secondary antibody (1/1000-fold dilution, Molecular Probes, Eugene, OR, USA) for 3 h at room temperature. Images were collected with a MRC-1024 laser-scanning microscope (Bio-Rad, Richmond, CA, USA) using ×4 or ×20 objective lenses. For comparisons of double-stained patterns, images were processed using Photoshop CS (Adobe Systems, Mountain View, CA, USA). High magnification images of the NeuN/active caspase-3/ssDNA/P-p38/P-JNK staining are shown for the cornu ammonis 1 (CA1) region, unless otherwise indicated.

Western blotting analysis of slices

Slices were homogenized in 100 μl lysis buffer (10 mM Tris, pH 7.5, 150 mM NaCl, 1 mM EDTA, 1 mM EGTA, 1% Triton X-100, 0.1% SDS, 1 mM sodium orthovanadate, 1% deoxycholate, and 10 μg/mL each aprotinin, bestatin, pepstatin A, leupeptin), using Tissue Lyser (Qiagen, Hilden, Germany). The proteins were separated in 10% SDS-PAGE gels and transferred to PVDF membranes. The membranes were blocked for 1 h in Tris-buffered saline containing 0.1% Tween-20 (TBS/T) and 5% non-fat dry milk at room temperature. Then the membranes were incubated with the primary antibody (1/1000-fold dilution in TBS/T containing 5% BSA) overnight at 4 °C. After three washes with TBS/T, the membranes were incubated with a horseradish peroxidase–conjugated anti-rabbit antibody (1/2000 dilution in TBS/T containing 5% non-fat dry milk) for 1 h at room temperature. The membranes were washed with TBS/T three times, and the proteins were visualized by chemiluminescence.

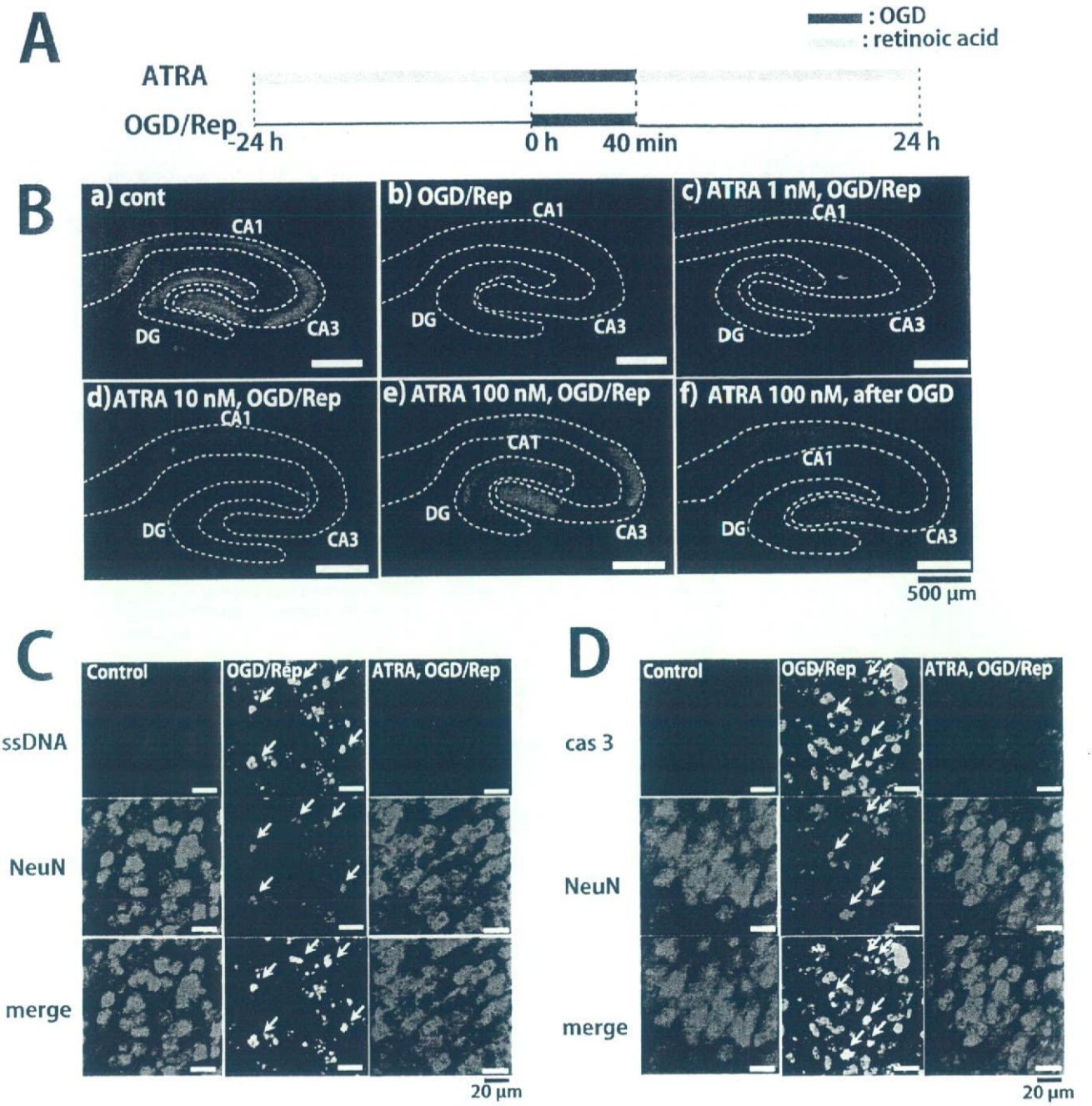

Fig. 1. The protective effect of ATRA on OGD/Rep-induced damage of neurons in the organotypic hippocampal slice culture. (A) A schematic diagram of the experimental protocol. Hippocampal slices were treated with ATRA 24 h before OGD and during Rep. The slices were subjected to OGD for 40 min followed by 24 h Rep. (B) The protective effect of ATRA on neurons in hippocampal slices. (a) NeuN staining of control slices. Incubation period for 12 days did not affect the NeuN staining of hippocampal slices. (b) OGD/Rep-induced neuronal loss. OGD/Rep dramatically decreased NeuN staining in hippocampal slices. (c–e) Effect of ATRA on the OGD/Rep-induced decrease of NeuN staining in hippocampal slices. At 1 nM, ATRA did not have a significant effect on NeuN staining decreased by OGD/Rep (c). At ≥10 nM ATRA prevented the decrease in NeuN by OGD/Rep (d, 10 nM; e, 100 nM). (f) The protective effect of ATRA after OGD. ATRA (100 nM) after OGD also had protective effects. Scale bar=500 μm. (C) DNA damage associated with the OGD/Rep-induced decrease in NeuN. In control, ssDNA signals were hardly detected (left, upper panel). OGD/Rep increased ssDNA signals (center, upper panel), which were shrunken and merged with NeuN signals (center, lower panel, arrows). ATRA prevented the changes in NeuN signals (right, middle panel) and reversed the increased ssDNA signals (right, upper panel). (D) OGD/Rep activates caspase-3 in neuronal cells. In control, the signals for active caspase-3 were barely detected (left, upper panel). OGD/Rep induced an increase in active caspase-3 (center, upper panel), which was colocalized with NeuN signals (center, arrows). ATRA prevented the OGD/Rep-induced changes in NeuN and active caspase-3 (right, middle and upper panels). Scale bar=20 μm.

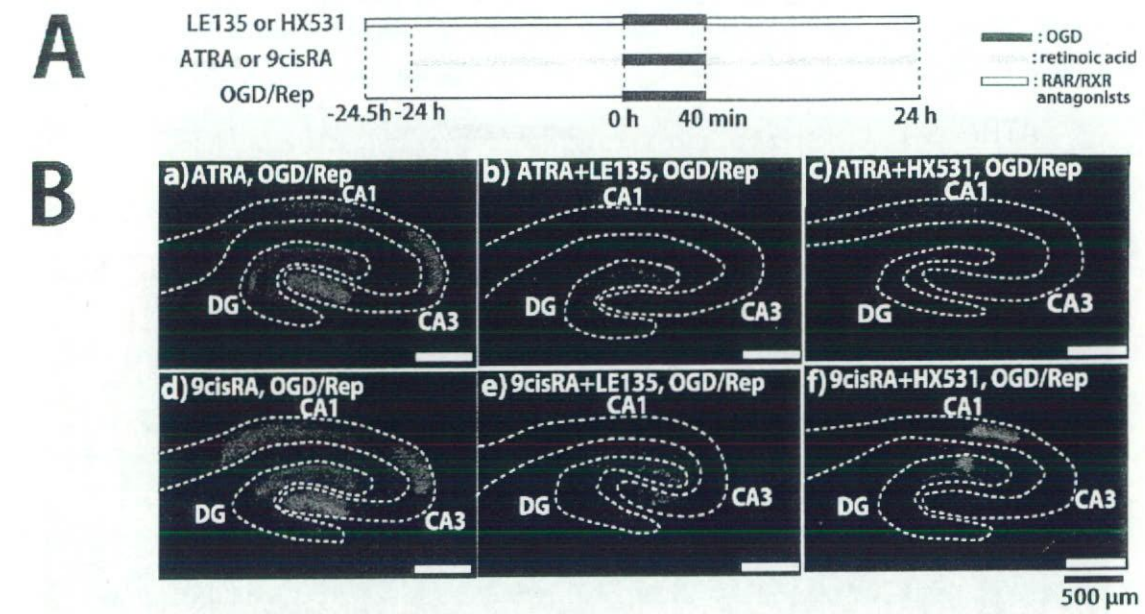

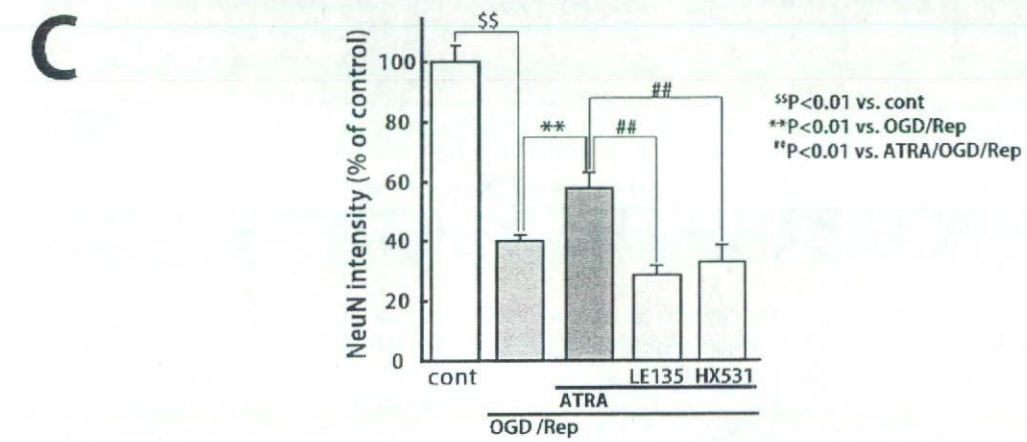

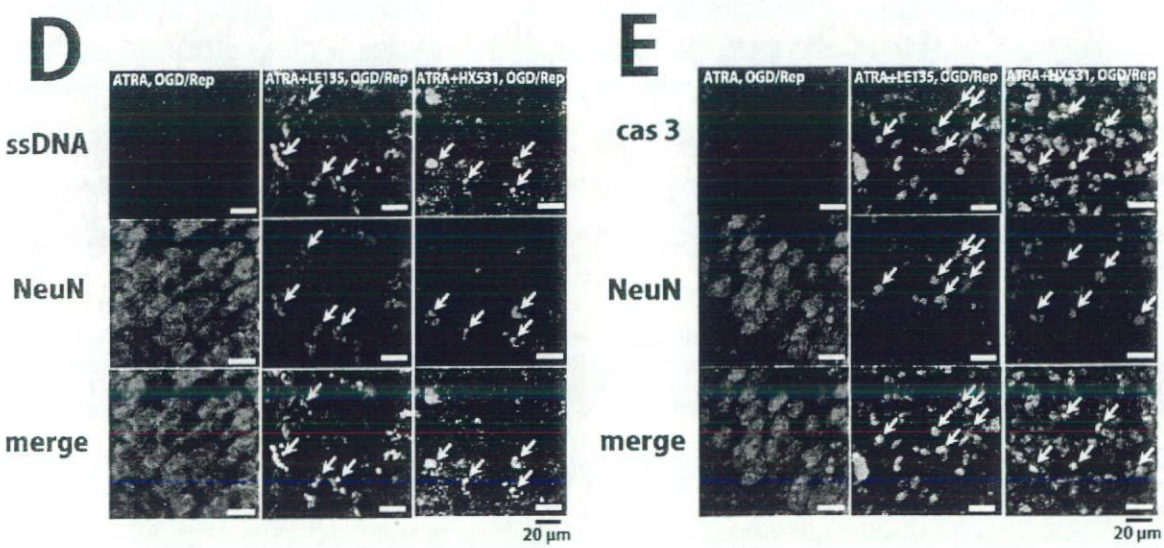

Fig. 2. The inhibitory effect of RAR/RXR antagonists on the RA-induced protective effect. (A) A schematic diagram of the experimental protocol. Hippocampal slices were treated with RAs (ATRA or 9-*cis* RA) 24 h before OGD and during Rep. Antagonists for RAR and RXR were added to the culture medium 30 min before and during RA treatment. The slices were subjected to OGD for 40 min and Rep for 24 h. (B) RAR/RXR antagonists inhibit the neuroprotective effect of RA. The effect of ATRA (a) was inhibited by both RAR antagonist LE135 (1 μM) (b) and RXR antagonist HX531

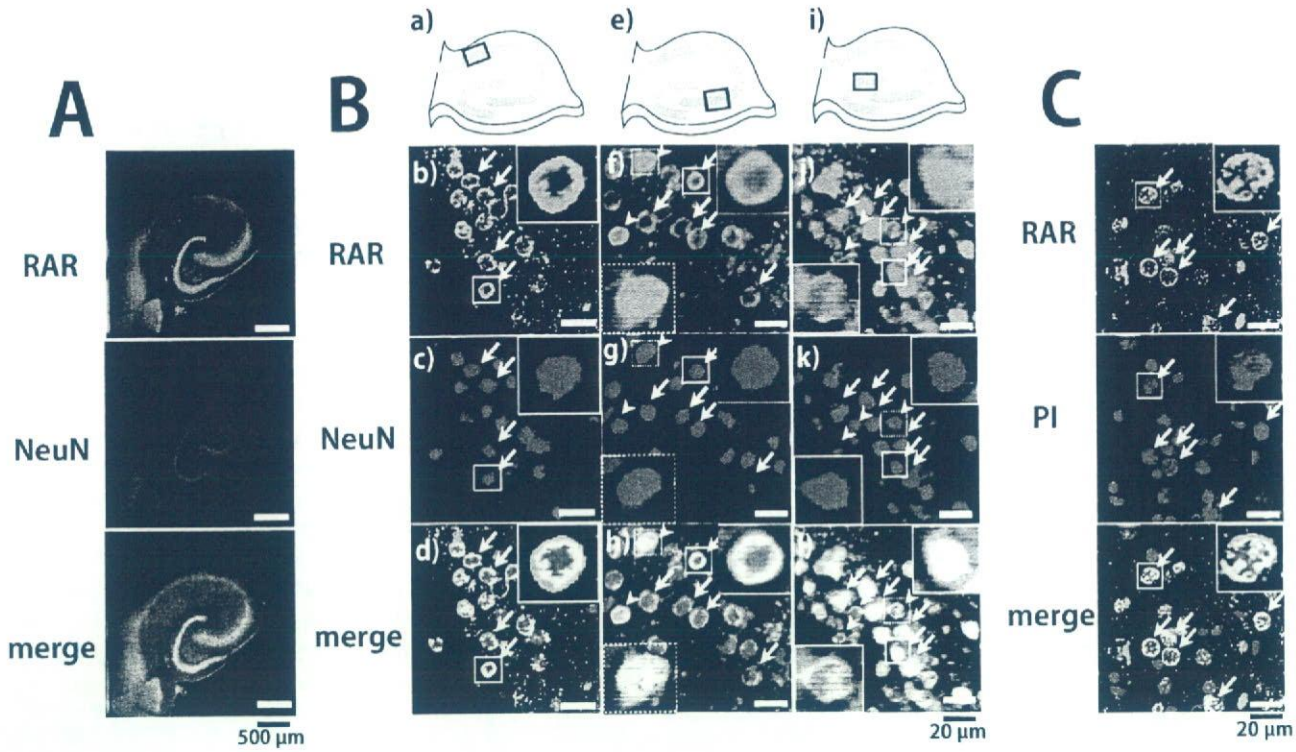

Fig. 3. Subregional expression pattern of RAR in the hippocampus. (A) Immunostaining for RAR showed a neuronal cell layer-like pattern in CA1 to CA3 and in DG (upper panel). The RAR signals were clearly colocalized with those for NeuN (lower panel). Scale bar=500 μm. (B) Differences in the expression pattern of RAR between subregions of the hippocampus. Images in b–d were obtained from the CA1 region indicated by the square in a. The signals for RAR appeared in ring-forms in CA1 (b; arrows). The signals for NeuN (c) were colocalized with those for RAR (d). Images in f–h were obtained from the CA3 region indicated by the square in e. In the CA3 region, RAR signals were mainly in ring-forms (f; arrows) but a few were in diffusion-forms (f; arrowheads), which were colocalized with those for NeuN (g, h). Images in j–l were obtained from the DG region indicated by the square in i. The RAR signals in DG were observed mainly in diffusion-forms (j; arrows) with a few RARs in ring-forms (j; arrowheads), which were colocalized with the NeuN signals (k, l). (C) RARs exist in the nucleus. RARs in CA1 were colocalized with PI signals (arrows). The insets show high-magnified images of square-selected region. Scale bar=20 μm.

Quantification of the immunostaining

The intensity of NeuN, which is not only a marker for neuronal nuclei but also for neuronal viability in hippocampus (Nakatomi et al., 2002; Liu et al., 2004; Gao et al., 2005), was quantified using Image J software (http://rsb.info.nih.gov/ij/) (Lyuksyutova, 2003; MacDonald, 2006). The center parts of the neuronal cell layers from CA1 to CA3 or dentate gyrus (DG) were traced and analyzed (analysis-measure) by "line selection from tool bar" and the NeuN intensity was measured by "Analysis-measure" from the menu bar. The mean value was employed as the intensity of the signal.

Statistics

Data were expressed mean±S.E.M. unless otherwise indicated. Data were analyzed for statistical significance by ANOVA followed by Student-Neuman-Keuls post hoc test. Significance was imparted at the $P<0.05$ level.

RESULTS

The protective effect of RA on OGD/Rep-induced neuronal loss of hippocampal slice

Fig. 1A shows the experimental procedure in the present study. The neuronal cell layer of hippocampal slice cultures 12 days after dissection from 11-day-old rats is shown in Fig. 1B(a). The neuronal cell layer was confirmed by immunohistochemistry using an antibody against NeuN. OGD for 40 min and Rep for 24 h shrank the NeuN signal, which also decreased its intensity significantly (Fig. 1B(b)). Hippocampal slices were treated with ATRA 24 h before OGD/Rep. The decrease in the NeuN signal intensity by OGD/Rep was prevented by ATRA at ≥10 nM (Fig. 1B(c–e)). In addition to the pre-treatment, post-treatment with ATRA

(1 μM) (c). 9-*cis* RA also showed the protective effect on neuronal cells against OGD/Rep-induced damage (d). The protective effect of 9-*cis* RA was inhibited by LE135 (1 μM) (e) and HX531 (1 μM) (f). Scale bar=500 μm. (C) Quantification of the signals for NeuN. OGD/Rep decreased the NeuN intensity to 40% of the controls, which was restored to 60% by ATRA (100 nM, 24 h). The effect of ATRA was offset by LE135 (1 μM) or HX531 (1 μM). Values were expressed as mean±S.E.M. ($n=6\sim8$). $^{\$\$}$ $P<0.01$ vs. control. ** $P<0.01$ vs. OGD/Rep. $^{\#\#}$ $P<0.01$ vs. ATRA/OGD/Rep. (D) RAR/RXR antagonists aggravate DNA damage of neurons. The ATRA-mediated inhibition of the OGD/Rep-increased ssDNA signals (left, upper panel) as well as on the shrinkage of NeuN (left, middle panel), was diminished in the presence of LE135 (1 μM; center) or HX531 (1 μM; right). Signals for NeuN were colocalized with ssDNA signals (lower panels, arrows). (E) RAR/RXR antagonists aggravate caspase-3 activation by OGD/Rep. The inhibitory effect of ATRA on the OGD/Rep-induced increase in active caspase-3 (left, upper panel) was diminished in the presence of LE135 (1 μM; center) or HX531 (1 μM; right). NeuN (middle panels) was colocalized with active caspase-3 (lower panels). Scale bar=20 μm.

after OGD was also cytoprotective (Fig. 1B(f)). As DNA damage is a marker of ischemia-induced neuronal cell death (Kawase et al., 1999) and caspase-3 activation (Chen et al., 1998), we employed antibodies for ssDNA and active caspase-3. In the negative controls without OGD/Rep, immunostaining for ssDNA was hardly detected (Fig. 1C left, upper panel). After the OGD/Rep, the immunostaining for ssDNA was significantly enhanced (Fig. 1C center, upper panel). The NeuN signals were detected in ssDNA-positive cells and shrunken (Fig. 1C center, arrows). ATRA prevented not only the increases in ssDNA signals but also the decrease in NeuN and its shrinkage (Fig. 1C right). Cells positive for active caspase-3 were detected after OGD/Rep but not in the controls without OGD/Rep (Fig. 1D, upper panels). The signals for active caspase-3 in the OGD/Rep group were colocalized with the NeuN signals. ATRA prevented caspase-3 activation, as well as the shrinkage of NeuN signals (Fig. 1D, right).

The inhibitory effect of selective RAR and RXR antagonists on the ATRA-induced neuroprotection against OGD/Rep

We next examined whether the protective effect of ATRA was mediated by RAR and/or RXR. Hippocampal slices were treated with ATRA 24 h before OGD and during Rep (Fig. 2A). Antagonists for RAR and RXR were added to the culture medium 30 min before ATRA treatment. As shown in Fig. 2B, both a specific RAR antagonist LE135 (1 μM) and a specific RXR antagonist HX531 (1 μM) inhibited the protective effect of ATRA (100 nM, 24 h) (Fig. 2B(b, c)). In addition, 9-*cis* RA (100 nM) had a protective effect against OGD/Rep-induced neuronal death (Fig. 2B(d)), which was reversed by LE135 (1 μM) or HX531 (1 μM) (Fig. 2B(e, f)). LE135 and HX531 alone did not attenuate the NeuN signal in hippocampal slices (data not shown). Based on quantitative analyses using the Image J program, OGD/Rep appeared to decrease the intensity of the NeuN signal to 40% of the controls (Fig. 2C). ATRA (100 nM) significantly inhibited the effect of OGD/Rep on the NeuN intensity, which was reversed by LE135 (1 μM) and HX531 (1 μM). To confirm that the effect on NeuN reflected the cytoprotective activity of ATRA, hippocampal slices were simultaneously stained with specific antibodies for NeuN, ssDNA and active caspase-3. As shown in Fig. 2D and E, LE135 and HX531 also offset the inhibitory effect of ATRA on the signal intensities for ssDNA and active caspase-3 in the slices treated with OGD/Rep. Thus, the intensities for ssDNA and active caspase-3 were negatively associated with the abundance of NeuN.

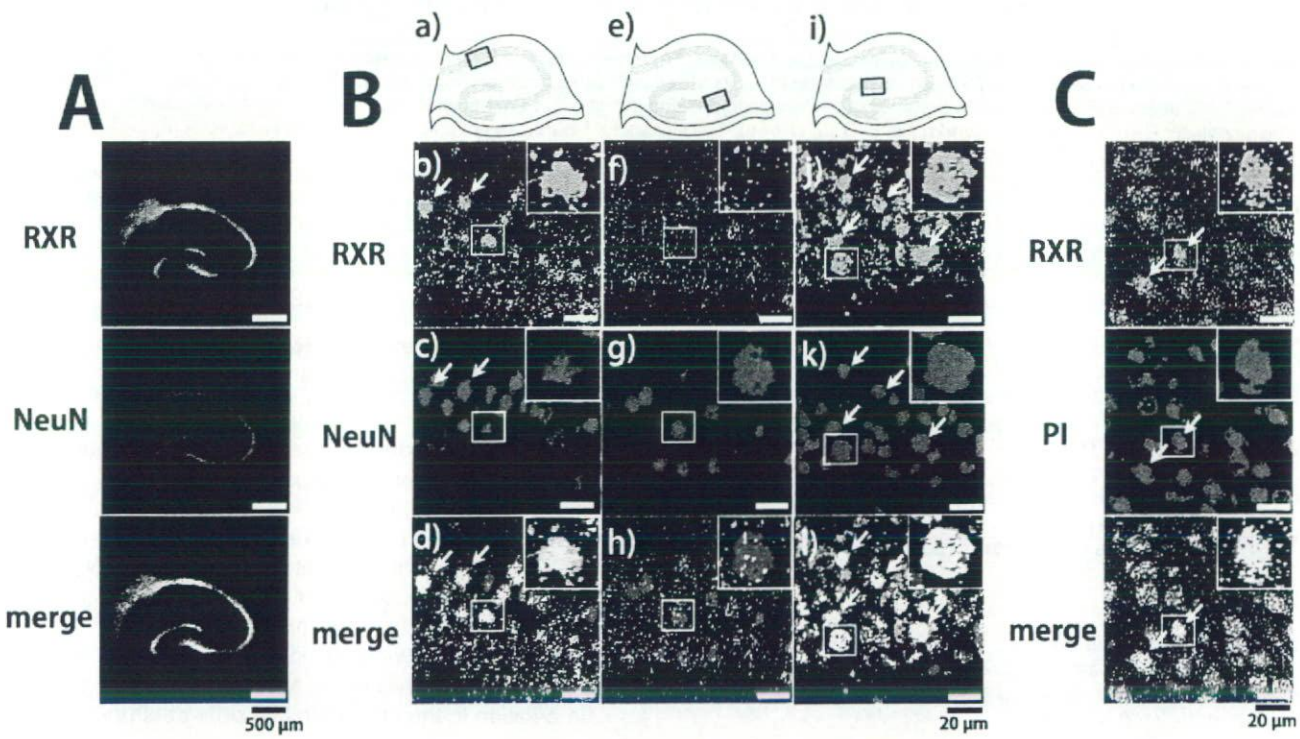

Fig. 4. Subregional expression pattern of RXR in the hippocampus. (A) Immunostaining for RXR showed neuronal cell layer-like pattern in CA1 to CA3 and in DG (upper panel). The signals for RXR were colocalized with those for NeuN (lower panel). Scale bar=500 μm. (B) Differences in the expression pattern of RXR between subregions of hippocampus. Images in b–d were obtained from the CA1 region indicated by the square in a. The signals for RXR appeared in diffusion-forms in CA1 (b; arrows). The signals for NeuN signals (c) were colocalized with those for RXR (d). Images of f–h were obtained from the CA3 region indicated by the square in e. In contrast to CA1, the RXR signals were barely detectable in CA3 (f), though they were colocalized with the NeuN signals (g, h). Images in j–l were obtained from the DG region indicated by the square in i. The RXR signals in DG were colocalized with those for NeuN (j–l, arrows). RXR-positive neurons were more frequent in DG, compared with CA1. (C) RXRs exist in the nucleus. RXRs in CA1 were colocalized with PI signals (arrows). The insets show highly magnified images of the square-selected region. Scale bar=20 μm.

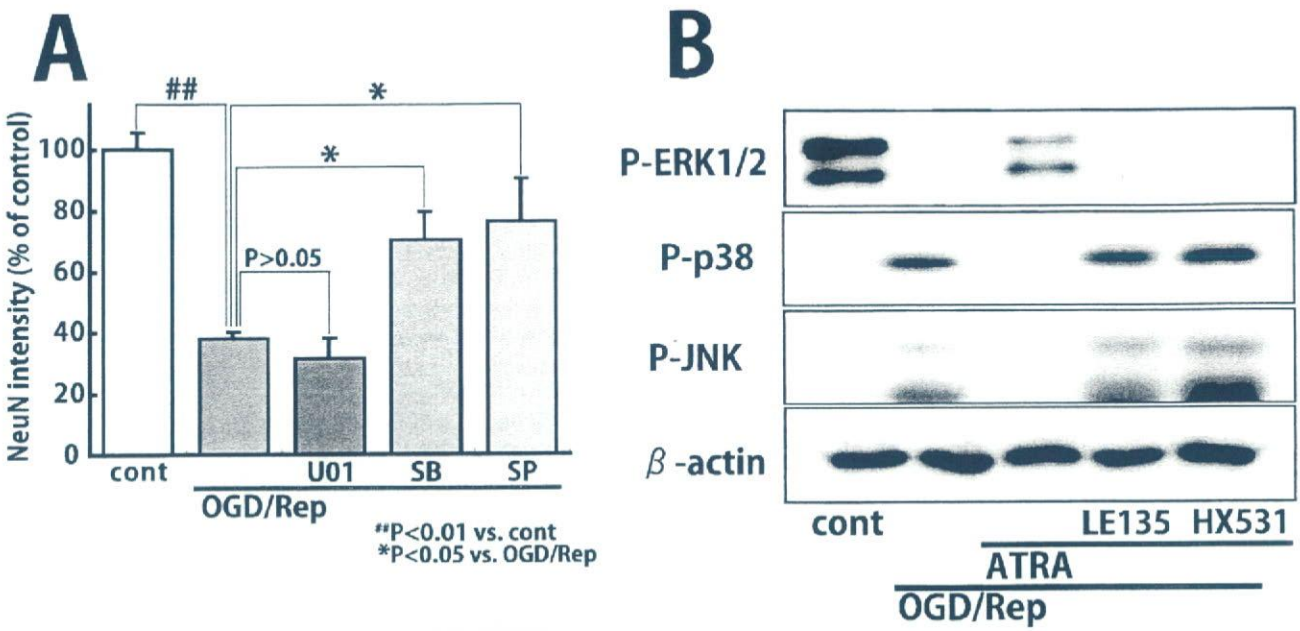

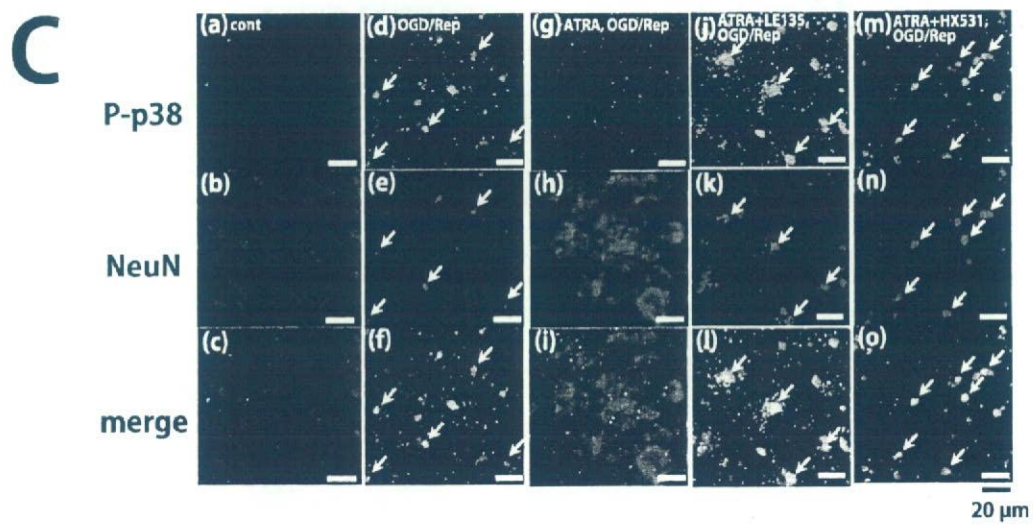

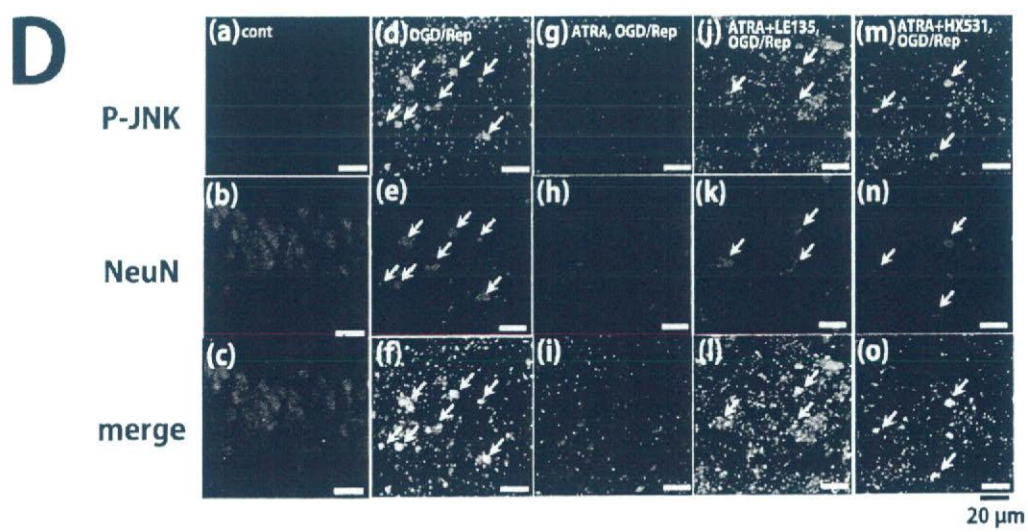

Fig. 5. (*Caption overleaf*)

Subregional differences of RAR and RXR expression in the hippocampus

To determine the expression of RAR and RXR in the hippocampus, we performed immunohistochemical analyses of the tissue slices using specific antibodies for RAR and RXR. In hippocampal slices fixed right after dissection from rat hippocampus, RAR was expressed in CA1 to CA3 and DG (Fig. 3A) and was colocalized with NeuN. Misner et al. (2001) have shown RA signaling activity in CA1, CA2, CA3 and DG of hippocampus, consistent with our results. RXR was also expressed in CA1 to CA3 and DG, and colocalized with NeuN (Fig. 4A). At higher magnification, subregional differences of RAR and RXR expression were observed in the hippocampus (Figs. 3 and 4). Diffused signals of RAR were observed in DG (Fig. 3B (j), arrows), and parts of them were in ring-formation (Fig. 3B(j), arrowheads). Almost all of RAR in square-selected region of CA3 (Fig. 3B(e)) were in ring-formation (Fig. 3B(f), arrows), and parts of them were in diffusion-forms (Fig. 3B(f), arrowheads). In the CA1 region, almost all of RARs were in ring-formation (Fig. 3B (b), arrows). The RXR signals from cells in CA1 and DG were dots diffused in the nucleus (Fig. 4B, arrows) and those in CA3 subregions were barely detectable (Fig. 4B, center). RAR and RXR were also colocalized with DNA-binding dye PI (Fig. 3C and Fig. 4C, arrows).

Inhibitory effect of ATRA on OGD/Rep-induced MAPK activation

As MAPKs have been associated with various physiological and pathological events including ischemia-induced neuronal cell death (Xia et al., 1995), we examined the role of MAPKs in the OGD/Rep-induced neuronal death, using specific inhibitors for subgroups of MAPK signaling. As shown in Fig. 5A, MEK1/2 (ERK kinase) inhibitor U0126 (10 μM) had no effect on the decrease in NeuN after OGD/Rep. In contrast, both a p38 inhibitor, SB203580 (20 μM), and a JNK inhibitor, SP600125 (20 μM), significantly prevented the OGD/Rep-induced decrease in NeuN. Both inhibitors protected not only CA1 but also CA3 neurons (data not shown), suggesting that the two kinases were activated in both subregions after OGD/Rep. Western blot analyses revealed that the OGD/Rep led to a decrease in P-ERK1/2 and increases in P-p38 and P-JNK. Pretreatment with ATRA (100 nM) prevented these changes in phosphorylated MAPKs, which were abolished in the presence of LE135 (1 μM) or HX531 (1 μM). To confirm whether OGD/Rep increased P-p38 and P-JNK in neuronal cells, immunohistochemical analyses were performed. In controls, signals for P-p38 and P-JNK were hardly detectable (Fig. 5C(a–c), 5D(a–c)), but seemed to exist in the cytoplasmic region. OGD/Rep enhanced the signals for both P-p38 and P-JNK, which were colocalized with the signals for NeuN (Fig. 5C(d–f), 5D(d–f), arrows). The NeuN signals were shrunk in OGD/Rep-treated slices, compared with the controls (Fig. 5C(b) and (e), 5D(b) and (e)). Pretreatment with ATRA (100 nM, 24 h) decreased the P-p38 and P-JNK signals, which were faintly detected around the NeuN signals (Fig. 5C(g–i) and 5D(g–i)). The shrinkage of the NeuN signal was also prevented by ATRA treatment. LE135 (1 μM) and HX531 (1 μM) inhibited the effects of ATRA (Fig. 5C(j–o), arrows and Fig. 5D(j–o), arrows).

DISCUSSION

In the present study, we demonstrated that ATRA induces a protective effect against OGD/Rep-induced damage in neurons from cultured hippocampal slices. The effect of ATRA was inhibited not only by a RAR antagonist but also by a RXR antagonist, indicating that ATRA-induced protection was mediated by RAR/RXR heterodimer. Selective RXR agonists and antagonists are known to synergistically enhance and inhibit activity of RAR in RAR/RXR heterodimers, respectively, and the opposite is observed in the case of RAR agonists and antagonists (Ebisawa et al., 1999). In the CA3 region, where ATRA had no neuroprotective activity, both a ring-formed and diffusion-formed distribution of RARs in the nucleus was found. However, a ring-formed as well as a diffuse-formed distribution of RARs mediated neuroprotection of ATRA in CA1 and DG, respectively, suggesting that the neuroprotective effect is independent of the pattern of RAR distribution. The signals for RXR were dots diffused in the nucleus. Unlike RAR that forms a heterodimer with RXR, RXR forms not only homo/heterodimers but also a homotetramer (Kersten et al.,

Fig. 5. The role of MAPK activation in the OGD/Rep-induced cell death of hippocampal neurons. (A) The effect of MAPK inhibitors on the OGD/Rep-induced decrease in NeuN. MEK1/2 inhibitor U0126 (10 μM) had no effect on the decrease in NeuN by OGD/Rep. Both p38 inhibitor, SB203580 (20 μM), and JNK inhibitor, SP600125 (20 μM), significantly inhibited the OGD/Rep-induced decrease in NeuN. All the MAPK inhibitors were added to the culture medium during Rep. Values were expressed as means ± S.E.M. of the fluorescent signal intensities for NeuN (n=3). (B) The effect of ATRA on OGD/Rep-induced changes in the levels of phosphorylated MAPKs. P-ERK1/2 was decreased by OGD/Rep, which was prevented by ATRA (100 nM, 24 h). The effect of ATRA on P-ERK1/2 was inhibited by LE135 (1 μM) or HX531 (1 μM). The increases in P-p38 and P-JNK, induced by OGD/Rep, were prevented by ATRA (100 nM, 24 h). The effects of ATRA on P-p38 and P-JNK levels were inhibited by LE135 (1 μM) or HX531 (1 μM). (C) Immunohistochemical analyses of p38 activation by OGD/Rep. In the controls, P-p38 was hardly detectable (a–c). The OGD/Rep led to an increase in the signals for P-p38 (d), as well as a shrinkage of the signals for NeuN (e; arrows). The P-p38 signals were colocalized with those for NeuN (f; arrows). The OGD/Rep resulted in the shrinkage of the NeuN signals (e; arrows). ATRA (100 nM, 24 h) prevented the increase in the P-p38 signals (g) and the shrinkage of the NeuN signals (h) after OGD/Rep. The effects of ATRA were inhibited by LE135 (1 μM) (j–l) or HX531 (1 μM) (m–o). The P-p38 signals were colocalized with signals for NeuN (l, o; arrows). (D) Immunohistochemical analysis of JNK activation by OGD/Rep. In the controls, P-JNK was hardly detectable in the NeuN-positive regions (a–c). In the areas of surrounding the NeuN signals, P-JNK signals were sparsely observed. P-JNK signals were significantly increased by OGD/Rep, which were colocalized with those for NeuN (d–f; arrows). ATRA (100 nM, 24 h) prevented the increase in P-JNK by OGD/Rep (g–i). The effect of ATRA was inhibited by LE135 (1 μM) (j–l) or HX531 (1 μM) (m–o). The P-JNK signals were colocalized with those for NeuN (arrows). ATRA (100 nM) was added to the slices 24 h before OGD and during Rep. LE135 (1 μM) and HX531 (1 μM) were added to the culture medium 30 min before ATRA treatment. Scale bar=20 μm.

1995). Such differences in the multimeric structure may lead to the difference in the pattern of receptor distribution. In contrast to RAR, RXR was barely expressed in the CA3 region. Therefore, the lack of the synergistic effect of RXR in CA3 may explain the subregional difference in the cytoprotective effect of ATRA. In addition, 9-*cis* RA, an agonist for both RAR and RXR, also showed no protective effect on CA3, suggesting a deficiency in the receptor heterodimer activity in this region. Furthermore, degradation rates of RAs in CA3 may also contribute to their subregion-selective effects, because the RA degrading enzyme CYP26B1 is known to be strongly expressed in the CA3 region (Abu-Abed et al., 2002). According to the report of Misner et al. (2001), endogenous retinoid signaling is active throughout the hippocampus (i.e. CA1–CA3 and DG). However, they also showed that the retinoid signaling activity is the most potent in the DG, followed by CA1 and hilus, and relatively low in CA3, which is consistent with our results.

We found that ATRA potently inhibited the increases in activated forms of p38 (P-p38) and JNK (P-JNK) after OGD/Rep, which was offset by RAR or RXR inhibitors. In addition, inhibition of JNK and p38 activity by their specific inhibitors prevented neuronal damage by OGD/Rep, indicating the death-promoting functions of JNK and p38 in OGD/Rep. These findings suggest that ATRA, acting through RAR/RXR, protects hippocampal neurons from OGD/Rep stress, at least partly, by preventing the activation of JNK and p38. ATRA is known to increase the expression of mitogen-activated protein kinase phosphatase-1 (MKP-1), protecting mesangial cells from H_2O_2-induced cell death by dephosphorylation and inactivation of JNK and p38 (Konta et al., 2001). Recently, MKP-1 was found to primarily dephosphorylate JNK and p38, but not ERK1/2 (Wu and Bennett, 2005). Therefore, upregulation of MKP-1 is one possible mechanism in the neuroprotective effects of ATRA, observed in the present study. Recent studies have shown that molecules generally called "nuclear receptors" (i.e. RXR, TR and steroid hormone receptors) elicit non-genomic effects in response to their agonists (Hiroi et al., 2006; Wehling and Losel, 2006; Moraes et al., 2007). Additionally, ATRA is known to phosphorylate neuronal ERK in a nongenomic manner (Canon et al., 2004), which is consistent with its inhibitory effect on OGD/Rep-mediated ERK dephosphorylation. In the present study, selective RAR or RXR antagonists inhibited the neuroprotection by ATRA. Furthermore, ATRA applied after OGD was also neuroprotective. Therefore, it is also possible that ATRA protected hippocampal slices from OGD/Rep-induced cell injuries via the non-genomic action of RAR or RXR.

In contrast to JNK and p38, ERK1/2 mediates the pro-survival functions in staurosporine-treated neurons (Zhu et al., 2002). It has been suggested that BDNF is the mediator for the pro-survival effect of ERK1/2 (Han and Holtzman, 2000). ATRA is known to upregulate Trk B, the receptor for BDNF, NT-3 and NT-4/5, facilitating BDNF signaling (Kaplan et al., 1993; Kobayashi et al., 1994). Although the inhibition of endogenous ERK1/2 activity by a MEK inhibitor did not facilitate cell death by OGD/Rep, ATRA inhibited an OGD/Rep-induced decrease in P-ERK1/2. Therefore, it is still possible that P-ERK1/2 also contributes to the neuroprotection of ATRA under OGD/Rep.

CONCLUSION

In conclusion, our results suggest that ATRA has a protective effect on hippocampal neurons against OGD/Rep-induced damages, by inactivating JNK and p38 via RAR/RXR heterodimers. As ATRA is a lipophilic molecule, orally applied ATRA can easily reach the CNS thorough blood–brain barrier (Crandall et al., 2004). Although relatively high concentrations of ATRA (10–100 nM) were necessary for the neuroprotection in our ex vivo model, they are achievable by an oral administration of ATRA not only in rats but also in humans in a clinical setting (Saadeddin et al., 2004; Muindi et al., 1992). Therefore, our findings provide new insights into clinical applications of ATRA for the treatment of CNS diseases such as stroke.

Acknowledgments—We thank Dr. Koichi Shudo for the gracious gift of LE135 and HX531, and we thank Tomoko Obama for technical assistance. We are grateful to Dr. Helen Kiriazis for critical reading of the manuscript. This study was partly supported by grants from National Institute of Biomedical Innovation (MF-16), from the Uehara Memorial Foundation, and from the Ministry of Health, Labor and Welfare of Japan, and grants-in-aid for Scientific Research (B) and (C), for Young Scientists (A) and on Priority Areas (A) from the Ministry of Education, Science, Sports and Culture of Japan.

REFERENCES

Abu-Abed S, MacLean G, Fraulob V, Chambon P, Petkovich M, Dolle P (2002) Differential expression of the retinoic acid-metabolizing enzymes CYP26A1 and CYP26B1 during murine organogenesis. Mech Dev 110:173–177.

Ahlemeyer B, Krieglstein J (1998) Retinoic acid reduces staurosporine-induced apoptotic damage in chick embryonic neurons by suppressing reactive oxygen species production. Neurosci Lett 246:93–96.

Behrens A, Sibilia M, Wagner EF (1999) Amino-terminal phosphorylation of c-Jun regulates stress-induced apoptosis and cellular proliferation. Nat Genet 21:326–329.

Boulton TG, Nye SH, Robbins DJ, Ip NY, Radziejewska E, Morgenbesser SD, DePinho RA, Panayotatos N, Cobb MH, Yancopoulos GD (1991) ERKs: a family of protein-serine/threonine kinases that are activated and tyrosine phosphorylated in response to insulin and NGF. Cell 65:663–675.

Canon E, Cosgaya JM, Scsucova S, Aranda A (2004) Rapid effects of retinoic acid on CREB and ERK phosphorylation in neuronal cells. Mol Biol Cell 15:5583–5592.

Chambon P (1994) The retinoid signaling pathway: molecular and genetic analyses. Semin Cell Biol 5:115–125.

Chambon P (1996) A decade of molecular biology of retinoic acid receptors. FASEB J 10:940–954.

Chen J, Nagayama T, Jin K, Stetler RA, Zhu RL, Graham SH, Simon RP (1998) Induction of caspase-3-like protease may mediate delayed neuronal death in the hippocampus after transient cerebral ischemia. J Neurosci 18:4914–4928.

Chiang MY, Misner D, Kempermann G, Schikorski T, Giguere V, Sucov HM, Gage FH, Stevens CF, Evans RM (1998) An essential

role for retinoid receptors RARbeta and RXRgamma in long-term potentiation and depression. Neuron 21:1353–1361.

Corcoran J, So PL, Maden M (2002) Absence of retinoids can induce motoneuron disease in the adult rat and a retinoid defect is present in motoneuron disease patients. J Cell Sci 115:4735–4741.

Crandall J, Sakai Y, Zhang J, Koul O, Mineur Y, Crusio WE, McCaffery P (2004) 13-cis-retinoic acid suppresses hippocampal cell division and hippocampal-dependent learning in mice. Proc Natl Acad Sci U S A 101:5111–5116.

de Urquiza AM, Liu S, Sjoberg M, Zetterstrom RH, Griffiths W, Sjovall J, Perlmann T (2000) Docosahexaenoic acid, a ligand for the retinoid X receptor in mouse brain. Science 290:2140–2144.

Ebisawa M, Umemiya H, Ohta K, Fukasawa H, Kawachi E, Christoffel G, Gronemeyer H, Tsuji M, Hashimoto Y, Shudo K, Kagechika H (1999) Retinoid X receptor-antagonistic diazepinylbenzoic acids. Chem Pharm Bull (Tokyo) 47:1778–1786.

Gao J, Duan B, Wang DG, Deng XH, Zhanf GY, Xu L, Xu TL (2005) Coupling between NMDA receptor and acid-sencind ion channel contributes to ischemic neuronal death. Neuron 48:635–646.

Goodman AB, Pardee AB (2003) Evidence for defective retinoid transport and function in late onset Alzheimer's disease. Proc Natl Acad Sci U S A 100:2901–2905.

Guyton KZ, Liu Y, Gorospe M, Xu Q, Holbrook NJ (1996) Activation of mitogen-activated protein kinase by H2O2. Role in cell survival following oxidant injury. J Biol Chem 271:4138–4142.

Han BH, Holtzman DM (2000) BDNF protects the neonatal brain from hypoxic-ischemic injury in vivo via the ERK pathway. J Neurosci 20:5775–5781.

Haskell GT, LaMantia AS (2005) Retinoic acid signaling identifies a distinct precursor population in the developing and adult forebrain. J Neurosci 25:7636–7647.

Herdegen T, Claret FX, Kallunki T, Martin-Villalba A, Winter C, Hunter T, Karin M (1998) Lasting N-terminal phosphorylation of c-Jun and activation of c-Jun N-terminal kinases after neuronal injury. J Neurosci 18:5124–5135.

Hiroi Y, Kim HH, Ying H, Furuya F, Huang Z, Simoncini T, Noma K, Ueki K, Nguyen NH, Scanlan TS, Moskowitz MA, Cheng SY, Liao JK (2006) Rapid nongenomic actions of thyroid hormone. Proc Natl Acad Sci U S A 103:14104–14109.

Hu BR, Wieloch T (1994) Tyrosine phosphorylation and activation of mitogen-activated protein kinase in the rat brain following transient cerebral ischemia. J Neurochem 62:1357–1367.

Ishikawa Y, Yokoo T, Kitamura M (1997) c-Jun/AP-1, but not NF-kappa B, is a mediator for oxidant-initiated apoptosis in glomerular mesangial cells. Biochem Biophys Res Commun 240:496–501.

Jacobs S, Lie DC, DeCicco KL, Shi Y, DeLuca LM, Gage FH, Evans RM (2006) Retinoic acid is required early during adult neurogenesis in the dentate gyrus. Proc Natl Acad Sci U S A 103: 3902–3907.

Kaplan DR, Matsumoto K, Lucarelli E, Thiele CJ (1993) Induction of TrkB by retinoic acid mediates biologic responsiveness to BDNF and differentiation of human neuroblastoma cells. Eukaryotic Signal Transduction Group. Neuron 11:321–331.

Kastner P, Mark M, Ghyselinck N, Krezel W, Dupe V, Grondona JM, Chambon P (1997) Genetic evidence that the retinoid signal is transduced by heterodimeric RXR/RAR functional units during mouse development. Development 124:313–326.

Kawase M, Fujimura M, Morita-Fujimura Y, Chan PH (1999) Reduction of apurinic/apyrimidinic endonuclease expression after transient global cerebral ischemia in rats: implication of the failure of DNA repair in neuronal apoptosis. Stroke 30:441–448; discussion 449.

Kersten S, Kelleher D, Chambon P, Gronemeyer H, Noy N (1995) Retinoid X receptor alpha forms tetramers in solution. Proc Natl Acad Sci U S A 92:8645–8649.

Kobayashi M, Kurihara K, Matsuoka I (1994) Retinoic acid induces BDNF responsiveness of sympathetic neurons by alteration of Trk neurotrophin receptor expression. FEBS Lett 356:60–65.

Konta T, Xu Q, Furusu A, Nakayama K, Kitamura M (2001) Selective roles of retinoic acid receptor and retinoid x receptor in the suppression of apoptosis by all-trans-retinoic acid. J Biol Chem 276:12697–12701.

Kuan CY, Whitmarsh AJ, Yang DD, Liao G, Schloemer AJ, Dong C, Bao J, Banasiak KJ, Haddad GG, Flavell RA, Davis RJ, Rakic P (2003) A critical role of neural-specific JNK3 for ischemic apoptosis. Proc Natl Acad Sci U S A 100:15184–15189.

Lee SR, Lo EH (2003) Interactions between p38 mitogen-activated protein kinase and caspase-3 in cerebral endothelial cell death after hypoxia-reoxygenation. Stroke 34:2704–2709.

Li Y, Hashimoto Y, Agadir A, Kagechika H, Zhang X (1999) Identification of a novel class of retinoic acid receptor beta-selective retinoid antagonists and their inhibitory effects on AP-1 activity and retinoic acid-induced apoptosis in human breast cancer cells. J Biol Chem 274:15360–15366.

Liu SH, Lau L, Wei JS, Zhu DY, Zou S, Sun HS, Fu YP, Liu F, Lu YM (2004) Expression of Ca^{2+}-permeable AMPA receptor channels primes cell death in transient forebrain ischemia. Neuron 43:43–55.

Lyukyutora AI, Lu CC, Milanesio N, King LA, Guo N, Wang Y, Nathans J, Tessier NM, Zou Y (2003) Anterior-posterior guidance of commissural axons by wnt-frizzled signaling. Science 302:1984–1988.

MacDonald JM, Beach MG, Porpiglia E, Cheehan AE, Watts RJ, Freeman MR (2006) The Drosophila cell corpse engulfment receptor draper mediates glial clearance of severed axons. Neuron 50:869–881.

Maden M (2001) Role and distribution of retinoic acid during CNS development. Int Rev Cytol 209:1–77.

Marshall CJ (1995) Specificity of receptor tyrosine kinase signaling: transient versus sustained extracellular signal-regulated kinase activation. Cell 80:179–185.

Misner DL, Jacobs S, Shimizu Y, de Urquiza AM, Solomin L, Perlmann T, De Luca LM, Stevens CF, Evans RM (2001) Vitamin A deprivation results in reversible loss of hippocampal long-term synaptic plasticity. Proc Natl Acad Sci U S A 98:11714–11719.

Mizukami Y, Yoshioka K, Morimoto S, Yoshida K (1997) A novel mechanism of JNK1 activation. Nuclear translocation and activation of JNK1 during ischemia and reperfusion. J Biol Chem 272: 16657–16662.

Moraes LA, Swales KE, Wray JA, Damazo A, Gibbins JM, Warner TD, Bishop-Bailey D (2002) Non-genomic signalling of the retinoid X receptor through binding and inhibiting Gq in human platelets. Blood 109:3741–3744.

Muindi JR, Frankel SR, Huselton C, DeGrazia F, Garland WA, Young CW, Warrell RP Jr (1992) Clinical pharmacology of oral all-trans retinoic acid in patients with acute promyelocytic leukemia. Cancer Res 52:2138–2142.

Namgung U, Xia Z (2000) Arsenite-induced apoptosis in cortical neurons is mediated by c-Jun N-terminal protein kinase 3 and p38 mitogen-activated protein kinase. J Neurosci 20:6442–6451.

Okuno S, Saito A, Hayashi T, Chan PH (2004) The c-Jun N-terminal protein kinase signaling pathway mediates Bax activation and subsequent neuronal apoptosis through interaction with Bim after transient focal cerebral ischemia. J Neurosci 24:7879–7887.

Saadeddin A, Torres-Molina F, Carcel-Trullols J, Araico A, Peris JE (2004) Pharmacokinetics of the time-dependent elimination of all-trans-retinoic acid in rats. AAPS PharmSci 6:E1.

Sahin M, Karauzum SB, Perry G, Smith MA, Aliciguzel Y (2005) Retinoic acid isomers protect hippocampal neurons from amyloid-beta induced neurodegeneration. Neurotox Res 7:243–250.

Segal RA, Greenberg ME (1996) Intracellular signaling pathways activated by neurotrophic factors. Annu Rev Neurosci 19:463–489.

Skrede KK, Westgaard RH (1971) The transverse hippocampal slice: a well-defined cortical structure maintained in vitro. Brain Res 35:589–593.

Strahan JE, Raimer S (2006) Isotretinoin and the controversy of psychiatric adverse effects. Int J Dermatol 45:789–799.